International Journal of Nanomedicine Dovepress

Open Access Full Text Article ORIGINAL RESEARCH

Bio-Inspired Nanodelivery Platform: Platelet Membrane-Cloaked Genistein Nanosystem for Targeted Lung Cancer Therapy

Rui Gao[1,*], Peihong Lin[1,*], Wenjing Yang[1,*], Zhengyu Fang[1], Chunxiao Gao[1], Bin Cheng[2], Jie Fang[3], Wenying Yu[1]

[1]School of Pharmacy, Hangzhou Medical College, Hangzhou, 310013, People's Republic of China; [2]Department of Traditional Chinese Medicine, Zhejiang Pharmaceutical University, Ningbo, 315500, People's Republic of China; [3]Zhejiang Provincial Laboratory of Experimental Animal's & Nonclinical Laboratory Studies, Hangzhou Medical College, Hangzhou, 310013, People's Republic of China

*These authors contributed equally to this work

Correspondence: Bin Cheng; Wenying Yu, Email 44418972@qq.com; zjyuwenying@163.com

Background: Genistein (Gen), a natural polyphenolic compound, has emerged as a promising candidate for lung cancer treatment. However, the potential clinical application of Gen is limited due to its poor solubility, low bioavailability, and toxic side effects. To address these challenges, a biomimetic delivery platform with cell membranes derived from natural cells as carrier material was constructed. This innovative approach aims to facilitate targeted drug delivery and solve the problem of biocompatibility of synthetic materials.

Methods: First, the liposomes (LPs) loaded with Gen (LPs@Gen) was prepared using the ethanol injection method. Subsequently, PLTM-LPs@Gen was obtained through co-extrusion after mixing platelet membrane (PLTM) and LPs@Gen. Additionally, the biological and physicochemical properties of PLTM-LPs@Gen were investigated. Finally, the targeting ability, therapeutic efficacy, and safety of PLTM-LPs@Gen for lung cancer were evaluated using both a cell model and a tumor-bearing nude mouse model.

Results: The optimal preparation ratio for LPs@Gen was Gen: soybean lecithin: cholesterol: DSPE-PEG2000 (3:30:5:10, mass ratio), while the ideal fusion ratio of LPs@Gen and PLTM was 1:1. The particle size of PLTM-LPs@Gen was 108.33 ± 1.06 nm, and the encapsulation efficiency and drug loading were 94.29% and 3.09% respectively. Gen was released continuously and slowly from PLTM-LPs@Gen. Moreover, PLTM-LPs@Gen exhibited good stability within one week. The results of in vitro cellular uptake and in vivo distribution experiments indicated that the carrier material, PLTM-LPs, has the immune escape ability and tumor targeting ability. Consequently, it showed better therapeutic effects than free drugs and traditional LPs in vitro and in vivo tumor models. In addition, safety experiments demonstrated that PLTM-LPs@Gen possesses good biocompatibility.

Conclusion: Biomimetic nanomedicine provides a new strategy for the precision treatment of lung cancer in clinical practice.

Keywords: bionic technology, platelet membrane, genistein, liposomes, lung cancer, targeted therapy

Introduction

Lung cancer, as one of the most prevalent malignant tumors globally,[1] has one of the highest mortality rate.[2] Currently, there exist primarily three drug therapy methods: chemotherapy, targeted therapy, and immunotherapy.[3] Chemotherapy remains the main treatment for lung cancer, but long-term or high doses of chemotherapy drugs can lead to drug resistance and systemic side effects.[4,5] Although targeted therapy and immunotherapy can selectively inhibit tumor cells and minimize adverse reactions, they are only applicable to certain patients with specific gene mutations.[6] Therefore, it is urgent to develop more efficient and safe treatments for lung cancer.

Genistein (Gen) is a kind of isoflavone compound (Figure 1) widely existing in legumes. Gen shows a significant inhibitory effect on various tumor cells.[7–9] Previous studies have confirmed that Gen can effectively inhibit the proliferation of A549 and H1975 cells in vitro, induce S-phase arrest of tumor cells, and subsequently promote

Received: 22 May 2024
Accepted: 24 September 2024
Published: 16 October 2024

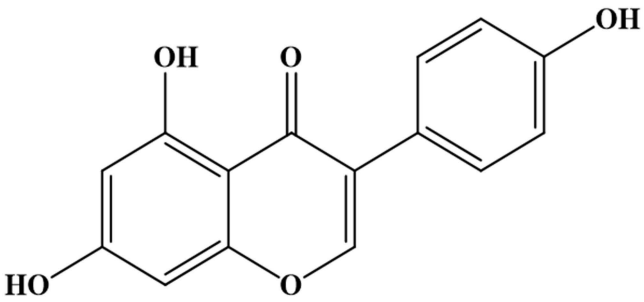

Figure 1 Chemical structure of Gen.

apoptosis.[10–12] It is suggested that Gen is a potential drug for the treatment of lung cancer. However, the clinical application of Gen is significantly limited due to its low solubility,[13] short half-life,[14] and poor targeting capabilities,[15] etc.

Nanotechnology has shown broad application prospects in the field of tumor treatment and diagnosis.[16] In the past, researchers have conducted extensive studies on various nanodelivery systems containing Gen, such as liposomes (LPs),[17] micelles emulsion,[15] and nanoparticles (NPs).[18] LPs has been widely studied and used due to its stable properties, good biocompatibility and high availability in tumor treatment.[19] Although LPs exhibits some passive targeting ability to tumor, a single passive targeting enables very limited enrichment of drugs at tumor sites.[20] In addition, LPs, as the foreign substance, is easily identified and cleared by the reticuloendothelial system in the body.[21–23] Therefore, how to help drugs achieve "immune escape" and "active targeting" has become the key to tumor therapy.

To address the aforementioned challenges, a biomimetic nanodelivery system based on cell membranes has been developed.[24] This functional coating utilizes natural biofilms as nanocarriers, combining the benefits of synthetic nanomaterials with biological entities. This innovative approach offers a novel solution for the issue of targeted drug delivery.[25,26] A large amount of experimental and clinical data shows platelets play an important role in the occurrence, development, invasion, and metastasis of tumors, which is mainly due to the interaction between tumor cells and platelet surface proteins. For instance, the high expression of CD44 protein in lung cancer cells, which has a high affinity with P-selectin protein on the platelet surface.[27] Moreover, the protein CD47 on platelet membrane (PLTM) prevents the drug modifying with PLTM from macrophage phagocytosis, thereby prolonging the circulation time of the drug in vivo.[28] Given the important physiological and pathological roles of platelets in the tumor environment, the PLTM-based drug delivery system may be a potential platform for targeted lung cancer therapy.

Therefore, in this paper, we constructed a biomimetic nanosystem, PLTM-LPs@Gen, with tumor-targeting capabilities by embedding PLTM into LPs loaded with Gen (Figure 2). To explore the application prospect of this nanodelivery platform, the lung cancer targeting ability, therapeutic efficacy, and safety of PLTM-LPs@Gen were evaluated by constructing an in vitro cell model and an in vivo nude mouse model with tumor. This work provides a novel strategy for the targeted delivery of clinical antitumor drugs.

Material and Methods

Materials

Human lung cancer A549 cells, lung adenocarcinoma H1975 cells, RAW264.7 cells and human umbilical vein endothelial cells (HUVEC) were purchased by Hangzhou Jcellm Biological Technology Co., Ltd.

BALB/c (nu/nu) nude mice, male, 6 weeks old, weighting 18–22 g, were provided by the Zhejiang Experimental Animal Center, experimental animal production license No. SCXK (Zhejiang): 2019–0002. All nude mice were raised in an SPF environment with a relative humidity of 55 ± 10%, temperature of 22 ± 2 °C, and light alternated between light and dark for 12 h. All animal care and experimental protocols (No. 2021–052) were approved by the Experimental Animal Ethics Committee of Hangzhou Medical College, and all in vivo experiments were conducted in accordance with the NIH Guide for the Care and Use of Laboratory Animals.

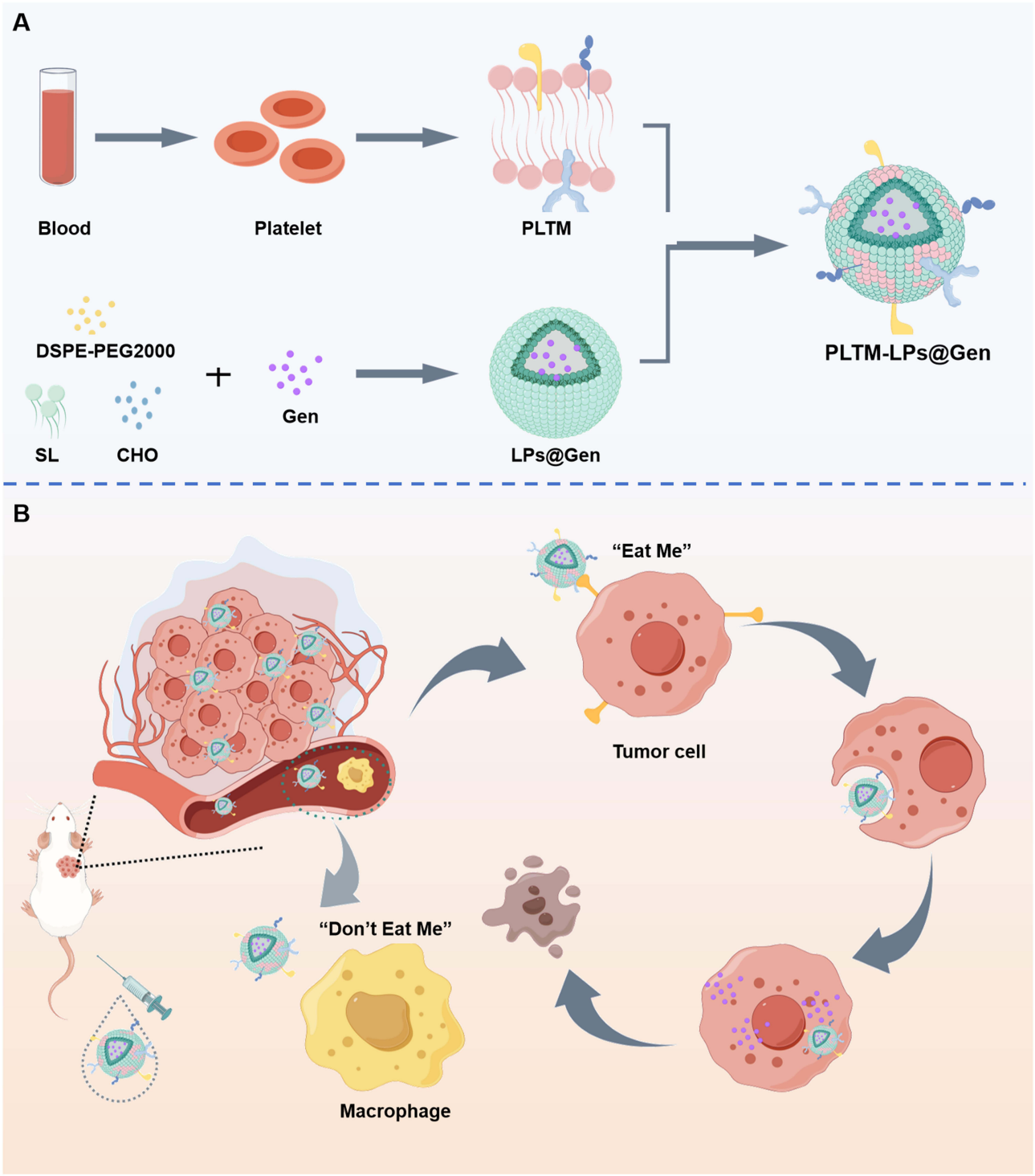

Figure 2 (**A**) Fabrication of PLTM-LPs@Gen. (**B**) Targeted therapy of lung cancer by PLTM-LPs@Gen. By Figdraw.

Gen (purity ≥ 98%) and FITC were obtained from Shanghai Aladdin Biochemical Technology Co., Ltd. Soybean lecithin (SL), cholesterol (CHO) and DSPE-PEG2000 were purchased from AVT (Shanghai) Pharmaceutical Technology Co., Ltd. DiO and DiD were obtained from Beijing Kulaibo Technology Co., Ltd. CD41 antibody was obtained from Abcam Plc (US), CD47 and CD62p antibodies were purchased from Proteintech (USA). DAPI was purchased from

Beijing Solarbio Science & Technology Co., Ltd. Cy5.5 was purchased from APE × BIO (USA). Annexin V-APC/PI apoptosis kit was obtained from Elabscience Biotechnology Co., Ltd. (Wuhan). All other reagents were analytically pure.

Preparation of LPs@Gen

LPs@Gen was prepared using the ethanol injection method.[29] Briefly, Gen, SL, CHO, and DSPE-PEG2000 (mass ratio: 3:30:5:10) were weighed in proportion and dissolved in 2 mL absolute ethanol. The mixture was slowly dropped into 10 mL PBS (pH 7.4) buffer with constant temperature (45 °C) and magnetic stirring (150 r). Once the ethanol was completely evaporated, the dispersion was then sonicated for 30 min in a water bath sonicator and passed through 0.80, 0.45, and 0.22 μm filters in turn. The final LPs@Gen product was stored at 4 °C.

Extraction and Purification of PLTM

PLTM was prepared according to the literature.[30] First, the whole blood was collected from ICR mice into anticoagulant tubes and centrifuged at 100 g for 20 min. The platelet-rich plasma in the upper layer was transferred to 2 mL centrifuge tubes, and PBS buffer containing 1 mm EDTA and 1% PMSF was added. The mixed solution was centrifuged (800 g for 20 min), then the supernatant was discarded, and PBS containing 1% PMSF was added for resuspension. The platelets were counted using an automatic blood cell counter. Subsequently, the purified platelets were repeatedly frozen and thawed at −80 °C for 3 times, then centrifuged (4000 g for 3 min) and washed with PBS containing 1% PMSF for 3 times to obtain PLTM.

Preparation of PLTM-LPs@Gen

The LPs@Gen and PLTM, prepared under specified conditions, were mixed in a predetermined mass ratio. After 10 min of ultrasound treatment in an ice bath, the mixture was successively coextruded through filtration membranes (0.80, 0.45, and 0.22 μm) to obtain PLTM-LPs@Gen.[31] Finally, PLTM-LPs@Gen was stored at 4 °C for future use.

Fluorescence Colocalization Analysis of PLTM-LPs@Gen

The fusion of PLTM and LPs@Gen was observed using a laser confocal microscopy to determine the optimal fusion ratio.[31,32] LPs@Gen was labeled with DiD, and PLTM was labeled with DiO and incubated on ice (both dye concentrations were 1 mmol · L^{-1}). After incubation for 10 min, DiO-labeled-PLTM and DiD-labeled-LPs@Gen were collected by centrifugation (12000 r, 10 min), respectively. Subsequently, the labeled LPs@Gen and PLTM were coextruded at different mass ratios (4:1, 2:1, 1:1, 1:2, and 1:4) through a LP extruder to form PLTM-LPs@Gen. The resulting fusion was detected through the colocalization of PLTM and LPs@Gen using laser confocal microscopy.

Particle Size, Zeta Potential, Morphology, and Stability of PLTM-LPs@Gen

The morphology of PLTM-LPs@Gen was observed via the transmission electron microscope (TEM). The particle size distribution and zeta potential of PLTM, LPs@Gen and PLTM-LPs@Gen were measured by a Mastersizer Nano-ZS90 laser particle size analyzer. PLTM-LPs@Gen was placed at 4 °C, and the initial stability was evaluated by measuring changes in particle size over the course of one week.

Drug Encapsulation and Loading Efficiency of PLTM-LPs@Gen

Ultrafiltration centrifugation was used to separate free drugs and membrane-chimeric LPs from PLTM-LPs@Gen.[15] Encapsulation efficiency (EE) and drug loading (DL) were determined by HPLC. HPLC conditions are described below: Diamonsil C18 column (4.6 mm × 250 mm, 5 μm), mobile phase: acetonitrile-0.1% phosphoric acid (55:45), flow rate: 1.0 mL · min^{-1}, column temperature: 30 °C, sample volume: 20 μL, and detection wavelength: 260 nm. The formulas for calculating EE and DL are as follows:

$$EE\% = \left(W - W_{free}\right)/W \times 100\% \quad (1)$$

$$DL\% = \left(W - W_{free}\right)/W_{all} \times 100\% \quad (2)$$

In the formulas, W_{free} is the free Gen content in the preparation, W is the total amount of Gen in the preparation, and W_{all} is the total amount of carrier and drug.

Membrane Protein Analysis of PLTM-LPs@Gen

The protein expression of the samples was analyzed using 10% sodium dodecyl sulphate-polyacrylamide gel electrophoresis (SDS-PAGE) and Western blot (WB).[33] The protein lysate was added into LPs@Gen, PLTM-LPs@Gen, and PLTM for pyrolysis, and the protein content of the above samples was determined by a BCA kit. After BCA protein quantification, loading buffer was added into the mixture, which was then boiled for 10 min and electrophoresed by SDS-PAGE. After protein separation, the gel was stained with Coomassie brilliant blue, and the protein expression was detected using a chemiluminescence imager. For WB analysis, proteins were transferred to a PVDF transfer membrane after electrophoresis. The membranes were blocked with 5% skim milk and incubated with primary antibodies followed by secondary antibodies. Next, membranes were subjected to a developer for imaging using chemiluminescence reagents. Finally, the expressions of specific membrane proteins CD41, CD62p, and CD47 in the samples were observed by a Bio-Rad chemiluminescence imaging system.

FT-IR Detection of PLTM-LPs@Gen

PLTM, LPs@Gen, and PLTM-LPs@Gen were freeze-dried, and the obtained powder samples were mixed with KBr powder. The FT-IR spectrum of each sample was obtained via the FT-IR spectrometer (Perkin Elmer, Frontier, USA).

In vitro Drug Release Behavior

The in vitro release of PLTM-LPs@Gen was investigated using the dialysis method.[34] A dialysis bag (MWCO: 8000–14000 Da) containing PLTM-LPs@Gen, LPs@Gen, or free Gen was placed in 50 mL of PBS (pH 7.4) buffer containing 0.5% (w/v) Tween 80 and oscillated in a thermostatic oscillator (37 °C, 100 r). A sample was collected at a fixed time point, and an equal amount of constant-temperature dissolution medium was added to maintain a constant volume. The Gen content was quantified using HPLC after filtering through a 0.45 μm membrane. The cumulative release rate of Gen was calculated according to Formulas (3) and (4):

$$Q_n = C_n V_n + \sum_{i=0}^{n-1} C_i V_i \tag{3}$$

$$\text{Release rate}\% = Q_n / W \times 100\% \tag{4}$$

In the formulas, Q_n is the total cumulative release of the drug, C_n is the drug concentration measured at t time, V_n is the total volume of the release medium, V_i is the volume of the sample taken out, C_i is the concentration measured at the time point before t time, and W is the total drug content of the sample.

Cell Killing Ability of PLTM-LPs@Gen

The cytotoxicity of free Gen, LPs@Gen, PLTM-LPs@Gen, and PLTM-LPs was assessed using the CCK-8 method. A549 and H1975 cells were inoculated into 96-well plates at 1×10^4 cells/well (n = 6) for 24 h and treated with various concentrations (5, 10, 20, 40, 80 μM) of Gen preparations.[35] After an additional 24 h, the cells were incubated with CCK-8 solution for 1 h, and the cell proliferation rate was determined by measuring the absorbance at 450 nm using a microplate reader. The survival rate was calculated according to Formula (5):

$$\text{Cell Viability}\% = (A_s - A_b)/(A_c - A_b) \times 100\% \tag{5}$$

In the formula, A_s is the absorbance of the experimental group, A_c is the absorbance of the control group, and A_b is the absorbance of the blank group.

Apoptosis Assay of PLTM-LPs@Gen

Apoptosis in A549 and H1975 cell lines was examined using Annexin V-APC/PI kit via flow cytometry.[36] Cells were inoculated into 6-well plates at 2×10^5 cells/well. After 24 h, the cells were treated with free Gen, LPs@Gen, or PLTM-LPs@Gen (Gen concentration: 40 μM) for an additional 24 h. Following treatment, the cells were collected, digested, and

washed, then stained with Annexin V-APC/PI according to the instructions. Apoptosis rates of the stained cells were determined by the flow cytometer.

In vitro Targeting Ability of PLTM-LPs

The in vitro tumor targeting ability of PLTM-LPs was evaluated via fluorescence microscopy.[37] First, the FITC preparations (free FITC, LPs-FITC, and PLTM-LPs-FITC) were prepared. A549 or H1975 cells were inoculated into 96-well plates at 1×10^4 cells/well and 12-well plates at 3×10^5 cells/well. The cells were treated with FITC preparations for 1, 2, and 4 h. The quantitative uptake of the three samples by the cells in the 96-well plate was detected via a microplate reader. The uptake of the three preparations by the cells was observed using fluorescence microscopy after the cells in the 12-well plates were fixed with paraformaldehyde, washed with PBS, stained with DAPI, and then washed again with PBS.

Immune Escape Ability of PLTM-LPs

Using RAW264.7 cells as the cell model, the immune escape ability of PLTM-LPs was investigated by a cell uptake test.[38] RAW264.7 cells were inoculated into 96-well plates and 12-well plates with 1×10^4 cells/well and 12-well plates at 3×10^5 cells/well. The subsequent procedures were conducted according to the previously described method titled "In vitro targeting ability of PLTM-LPs".

Establishment of Lung Cancer Transplant Tumor Model

A549 cells in the logarithmic growth phase were utilized in modeling. After digestion with pancreatic enzymes and centrifugation, the cells were resuspended in PBS (cell density was 2×10^7/mL) and placed on ice to reduce cell metabolism to maintain cell activity. Then, 2×10^6 cells per nude mouse were subcutaneously inoculated on the right side 1–2 cm away from the armpit, and subsequent tests could be performed once the tumor volume was about 100 mm^3. The tumor volume was calculated according to Formula (6):

$$V = L \times W^2/2 \tag{6}$$

In the formula, V is the tumor volume, L is the length of the tumor, and W is the width of the tumor.

In vivo Targeting Distribution of PLTM-LPs

In vivo imaging of small animals was employed to assess the targeting capability of PLTM-LPs.[39] The Cy5.5 preparations (LPs-Cy5.5 and PLTM-LPs-Cy5.5) were injected into nude mice with tumor via the tail vein. At 1, 6, 24, 30, and 48 h after injection, the fluorescence intensity of tumor sites was observed via a small animal imaging instrument. At 48 h, all nude mice were euthanized, and the heart, liver, spleen, lungs, kidneys, and tumors were harvested and placed in the imaging system to capture and record the signal intensity. Subsequently, the fluorescence intensity of each site was quantitatively analyzed.

In vivo Pharmacodynamic Evaluation of PLAM-LPs@Gen

To evaluate the therapeutic effect of different preparation groups on A549 tumor-bearing nude mice, tumor-bearing nude mice with tumor of about 100 mm^3 were selected on the 10th day after inoculation and randomly divided into four groups (n = 5). These tumor-bearing nude mice were treated with normal saline, free Gen, LPs@Gen, and PLTM-LPs@Gen through tail vein at a dosage of 20 mg/kg,[40] once every two days for a total of seven treatments. Tumor growth was measured and counted before each administration, and weight changes were monitored. The nude mice were euthanized three days after the cessation of treatment to collect tumor tissues for subsequent measurement of weight and volume.

The collected tumor tissues were fixed in paraformaldehyde and embedded in paraffin. Subsequently, the tumor tissues were sliced and analyzed using H&E and TUNEL staining. The necrosis and apoptosis of tumor cells among the different preparation groups were observed under a microscope.

Cytotoxicity of PLTM-LPs and PLTM-LPs@Gen

HUVEC were used as model cells to investigate the cytotoxicity of PLTM-LPs and PLTM-LPs@Gen. The 96-well plates were inoculated with 5×10^3 HUVEC per well. After 24 h of incubation, the cells were treated with PLTM-LPs and PLTM-LPs@Gen at the same concentrations of carrier materials (0, 25, 50, 100, 200, and 400 $\mu g \cdot mL^{-1}$) for 24 h. After addition of CCK-8, the absorbance was measured using a microplate reader, and the cell viability was subsequently calculated.

In vitro Hemolysis Test

The whole blood collected from mouse eyeballs was centrifuged, washed, and diluted in normal saline to obtain 2% erythrocyte suspension.[41] The Normal saline group was used as the negative control, and the Distilled water group was used as the positive control. Erythrocyte suspension was mixed with free Gen, LPs@Gen, and PLTM-LPs@Gen (Gen: 100, 200, 400, 800, 2000 μM) and incubated in a constant-temperature water bath at 37 ± 0.5 °C for 30 min, centrifuged at 1800 r for 10 min. At the same time, the supernatant was absorbed, and the absorption value of the sample at 575 nm was measured by UV to calculate hemolysis rate (>5% indicates hemolysis).

In vivo Safety Evaluation

Male healthy BALB/c mice were divided into the five groups (n = 5): Normal saline group, PLTM-LPs group, Free Gen group, LPs@Gen group, and PLTM-LPs@Gen group. The mice were given the drug once every two days by tail vein injection for seven times. After the administration, blood samples were collected from the eyeball for hematological analysis and assessment of liver and kidney function indices. Thrombin time (TT) and activated partial thrombin time (APTT) were selected as coagulation indices; blood urea nitrogen (BUN) and creatinine (CR) were chosen as indicators of renal function; aspartate aminotransferase (AST) and alanine aminotransferase (ALT) were selected as indicators of liver function. Finally, the heart, liver, spleen, lungs, and kidneys were removed and fixed with paraformaldehyde, and a histological analysis was performed after H&E staining.

Statistical Methods

Data analysis and mapping were performed using Graph Padprism 9.0 software. The analysis results were expressed mean ± SD, *T*-test or ANOVA were used for comparison between groups. $P < 0.05$ was considered statistically significant ($*p < 0.05$, $**p < 0.01$, $***p < 0.001$, and $****p < 0.0001$), ns represented nonsignificant difference.

Results

Preparation and Characterization of PLTM-LPs@Gen

To prepare PLTM-LPs@Gen, LPs containing Gen (LPs@Gen) was first prepared using the ethanol injection method.[29] Subsequently, platelets were isolated from the blood of ICR mice through gradient centrifugation. PLTM was then obtained by repeated freeze-thawing and ultrasonic purification of platelets according to the previously reported method.[31] Finally, PLTM-LPs@Gen was obtained by mixing, incubating and co-extruding LPs@Gen and PLTM.

To determine which ratio made LPs@Gen and PLTM blend together better, five ratios were set to conduct the fluorescence colocalization detection of LPs@Gen and PLTM. The results are shown in Figure 3. Compared to other groups, when the mass ratio of PLTM to LPs@Gen was 1:1, PLTM-LPs@Gen had significant red and green fluorescence colocalization, indicating PLTM and LPs@Gen were successfully chimed together. Therefore, the formulation was prepared with the mass ratio of PLTM to LPs@Gen 1:1 for subsequent experimental study.

The EE and DL of PLTM-LPs@Gen determined by HPLC were 94.29% and 3.09%, respectively. The TEM results (Figure 4A) reveal that LPs@Gen (left) and PLTM-LPs@Gen (right) had a round appearance with a uniform particle distribution. The particle size of PLTM-LPs@Gen was larger than that of LPs@Gen, and the coating structure could be observed, indicating that PLTM was evenly embedded on LPs@Gen. The results of the laser particle size analyzer show the particle size distributions of LPs@Gen and PLTM-LPs@Gen were 87.28 ± 1.69 nm and 108.33 ± 1.06 nm, respectively (Figure 4B). The embedding of PLTM on LPs@Gen may have contributed to the increase in particle size,

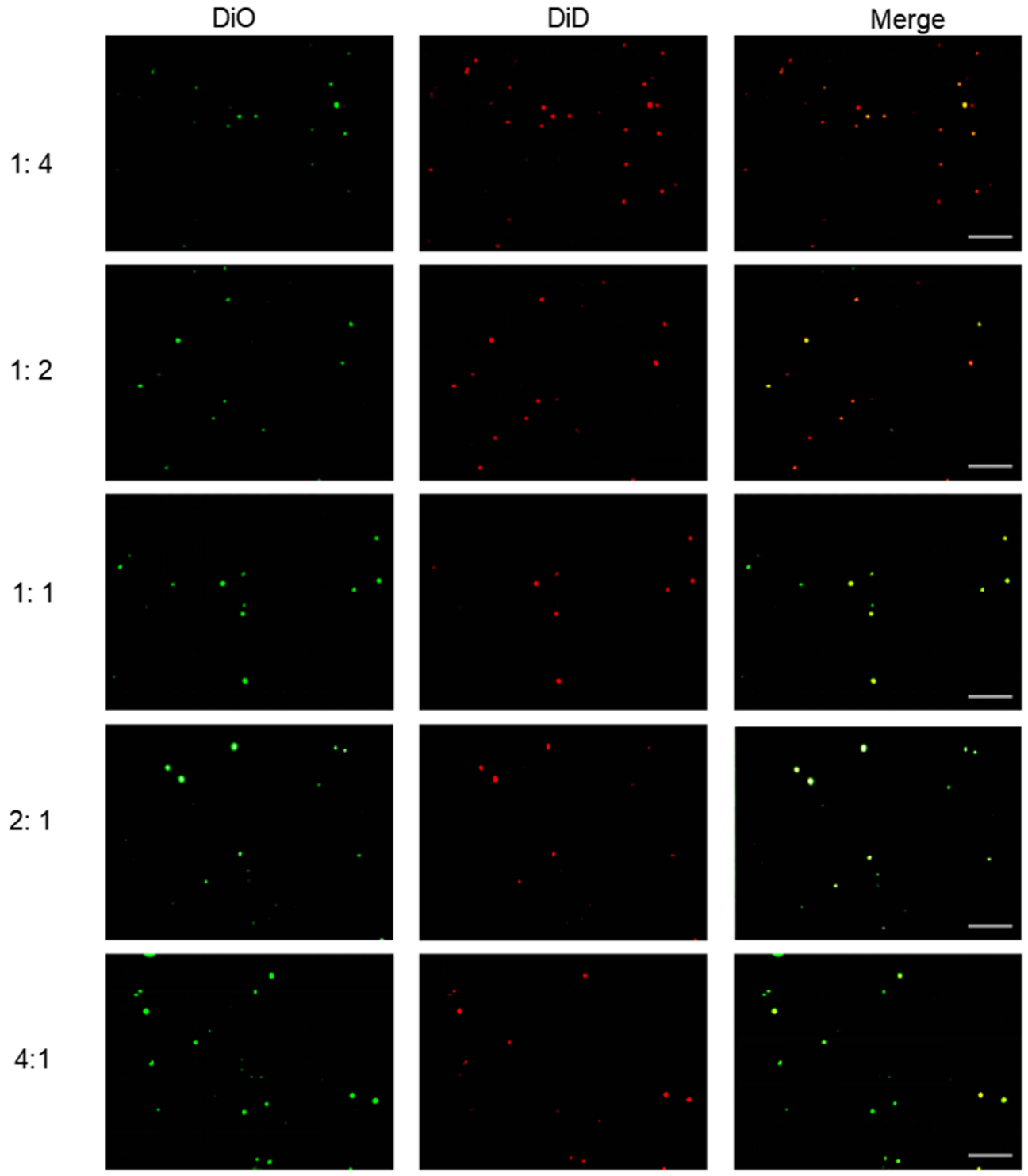

Figure 3 Colocalization of PLTM and LPs@Gen (scale bar, 10 μm).

which is consistent with the TEM results. Due to the high negative charge density of the cell membrane, the electronegativity of PLTM-LPs@Gen was enhanced compared to that of LPs@Gen (Figure 4C), resulting in a more stable nanosystem overall. Furthermore, the particle size of PLTM-LPs@Gen showed no significant change over a period of seven days (Figure 4D), suggesting that PLTM-LPs@Gen possesses good stability.

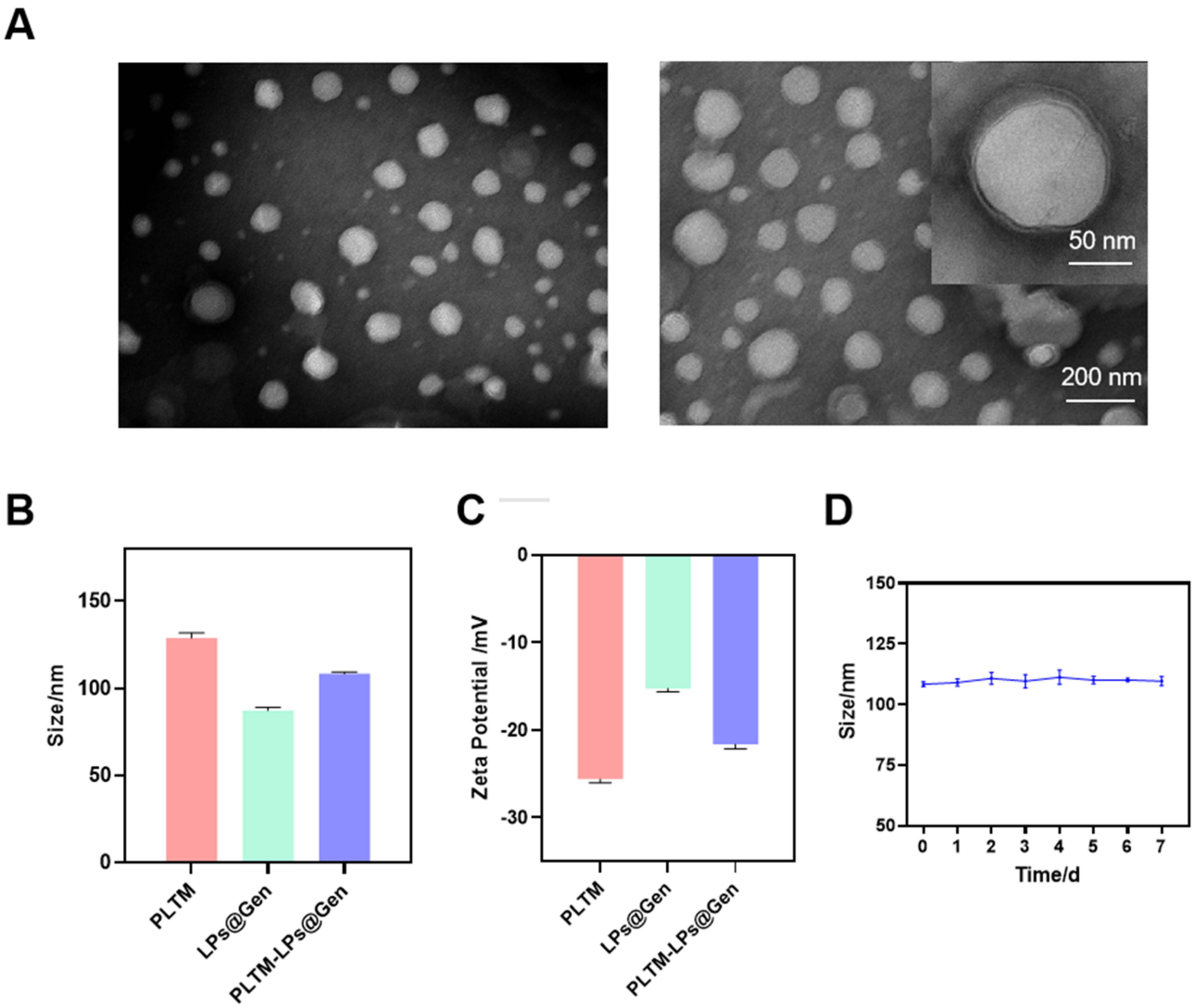

Figure 4 (**A**) TEM images of LPs@Gen (left) and PLTM-LPs@Gen (right). (**B**) Particle size results of PLTM-LPs@Gen. (**C**) Zeta potential results of PLTM-LPs@Gen. (**D**) Particle size change curve of PLTM-LPs@Gen.

To investigate whether the membrane protein on the surface of PLTM could be transferred to the surface of LPs@Gen under the preparation conditions of this study, the expression of total protein on PLTM-LPs@Gen was determined using SDS-PAGE. The results (Figure 5A) show that PLTM-LPs@Gen was consistent with the protein present on PLTM, while the negative control LPs@Gen did not express any protein, indicating that PLTM and LPs@Gen were successfully fused without significant protein damage during the preparation. On this basis, WB was used to further analyze the specific membrane proteins on PLTM-LPs@Gen. CD41, a signature protein in PLTM membrane, plays a vital role in coagulation. CD62p specifically recognizes and binds to CD44 on the surface of a cancer cell membrane. CD47 confers the ability of PLTM-LPs@Gen immune escape. As shown in Figure 5B, CD41, CD62p, and CD47 were expressed in PLTM and PLTM-LPs@Gen, but not in LPs@Gen. This indicates that PLTM-LPs@Gen retained the specific proteins of PLTM, thereby endowing it with the biological functions associated with PLTM.

To further prove the success of the bionic vector preparation, infrared detection of PLTM, LPs@Gen, and PLTM-LPs @Gen was conducted. The FT-IR results (Figure 5C) show related protein peaks in PLTM-LPs@Gen and extracted PLTM. A prominent peak corresponding to C-O-C stretching vibrations, attributed to the associated glycogroups in the PLTM film, was clearly observed at 1168 cm^{-1} in the spectrum of PLTM-LPs@Gen. In addition, a peak attributed to the protein amide I band at 1670 cm^{-1} was detected in the FT-IR spectra of both PLTM-LPs@Gen and PLTM. These results

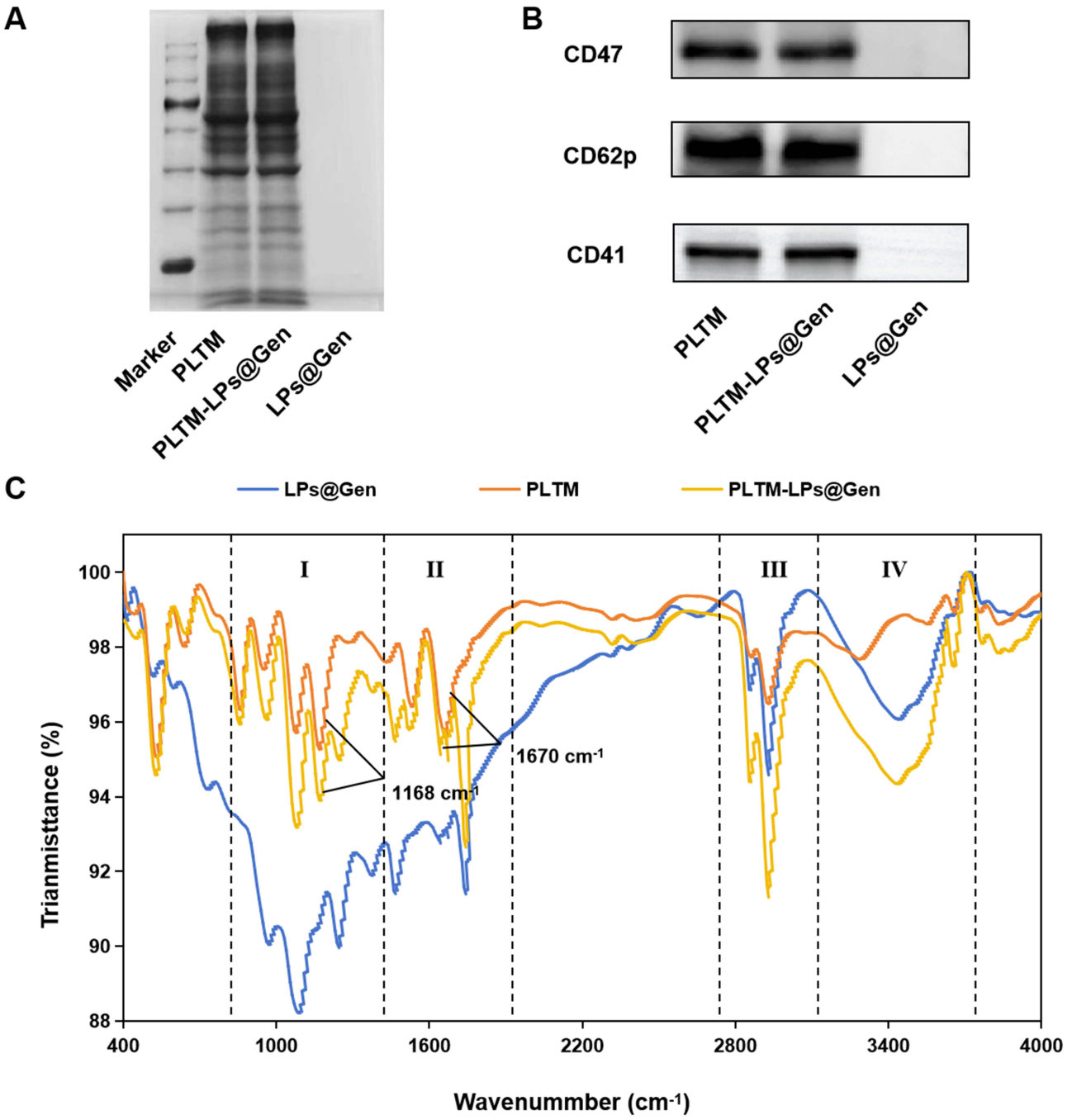

Figure 5 (**A**) SDS-PAGE results of whole protein expression. (**B**) Expression of characteristic proteins of WB. (**C**) FT-IR spectra of PLTM, LPs@Gen, and PLTM-LPs@Gen (I. phosphate and carbohydrate region; II. amide bands; III. C-H lipid stretch; IV. O-H and N-H stretch).

indicate that PLTM was successfully incorporated onto LPs, which is essential for PLTM-LPs@Gen to effectively target tumor sites.

In vitro Release Behavior of PLTM-LPs@Gen

The release behavior of Gen in PBS (pH 7.4) containing 0.5% (w/v) Tween 80 was investigated. The results of the in vitro drug release from PLTM-LPs@Gen are presented in Figure 6. Under this release condition, the Free Gen group exhibited rapid drug release, with 90.68% of the drug released after 4 h. In contrast, the LPs@Gen and PLTM-LPs@Gen groups demonstrated slower drug release rates. At 4 h, the cumulative drug release rates of the LPs@Gen and the PLTM-

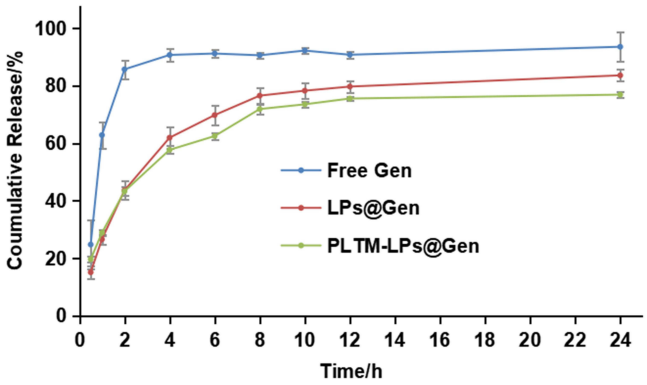

Figure 6 Release curve of PLTM-LPs@Gen.

LPs@Gen groups were 61.91% and 57.68%, respectively. By 24 h, drug release was completed in the Free Gen group, while 83.59% and 76.88% of the drug had been released in the LPs@Gen and PLTM-LPs@Gen groups, respectively. These findings indicate that PLTM-LPs could confer a sustained release effect for Gen in vitro. In addition, to explore the release mechanism of Gen, the release curve of PLTM-LPs@Gen was fitted to various models. The results (Table 1) show that the drug release behavior of PLTM-LPs@Gen had the highest fitting degree with the Weibull model (R^2 = 0.9548). These findings establish a foundation for subsequent cell and animal experiments of PLTM-LPs@Gen.

In vitro Anticancer Assay of PLTM-LPs@Gen

To evaluate the effect of PLTM-LPs@Gen on lung cancer in vitro, we assessed the viability and apoptosis of A549 and H1975 cells. The cytotoxic effects of the three groups of Gen preparations are illustrated in (Figure 7A and B). As the concentration of Gen increased, all drug intervention groups exhibited a significant inhibitory effect on A549 and H1975 cells, confirming the anti-lung cancer properties of Gen.[42] Compared with the Free Gen and LPs@Gen groups, the PLTM-LPs@Gen group showed the strongest inhibitory effect. At a Gen concentration of 40 μM, PLTM-LPs@Gen inhibited 63.55% and 71.25% of A549 and H1975 cells, respectively. When the Gen concentration reached 80 μM, the inhibition rates of PLTM-LPs@Gen on both lung cancer cell lines exceeded 90%.

As illustrated in (Figure 7C and D), the cytotoxic effects of PLTM-LPs@Gen became increasingly pronounced with prolonged treatment duration, surpassing those observed with free Gen. Furthermore, the cytotoxicity assessments of the blank carrier reveal no significant differences between the cells treated with PLTM-LPs and the untreated control (Figure 7E and F), indicating that the carrier material exhibits minimal toxicity towards tumor cells. Additionally, we assessed the capacity of each formulation to induce apoptosis in tumor cells. In both cell lines examined, PLTM-LPs@Gen demonstrated a comparable

Table 1 Release Fitting Equation for PLTM-LPs@Gen

Model	Equation	Correlation Coefficient (R^2)
Zero order processes	Q = 0.0216 t + 0.3903	0.5987
First order processes	ln (1-Q) = −0.0514 t - 0.5184	0.7043
Higuchi	Q = 0.1415 $t_{1/2}$ + 0.2134	0.8135
Ritger-Peppas	ln Q = 0.3711 lnt - 1.2073	0.9244
Weibull distribution	ln (1/1-Q) = 0.5276 lnt - 1.0175	0.9548

Abbreviations: Gen, Genistein; LP, Liposome; NP, Nanoparticle; PLTM, Platelet membrane; HUVEC, Human umbilical vein endothelial cells; SL, Soybean lecithin; CHO, Cholesterol; TEM, Transmission electron microscope; EE, Encapsulation efficiency; DL, Drug loading; SDS-PAGE, Sulphate-polyacrylamide gel electrophoresis; WB, Western blot; TT, Thrombin time; APTT, Activated partial thrombin time; BUN, Blood urea nitrogen; CR, Creatinine; AST, Aspartate aminotransferase; ALT, Alanine aminotransferase.

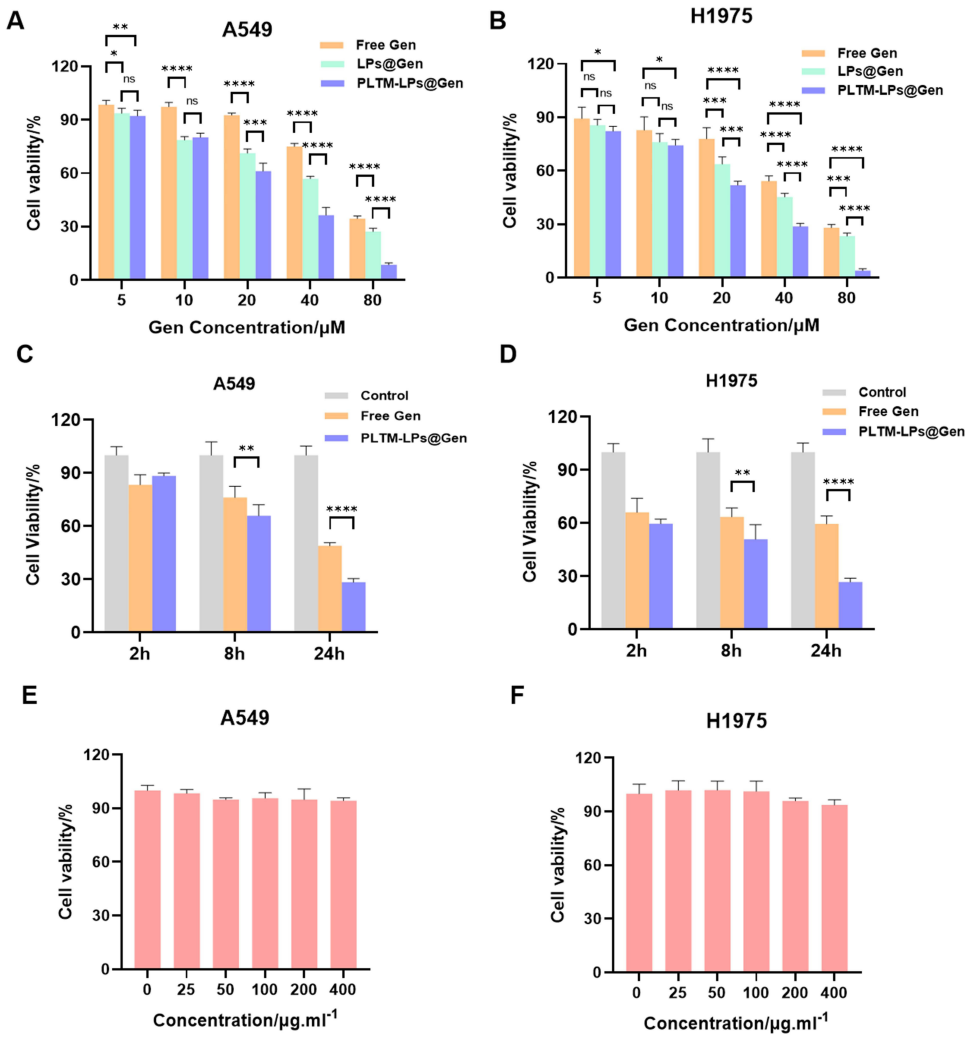

Figure 7 Effect of different Gen preparations on the viability of the A549 (**A**) and H1975 (**B**) cells. Toxicity of different Gen preparations on A549 (**C**) and H1975 (**D**) at 2, 8, 24 h. Effect of PLTM-LPs on A549 (**E**) and H1975 (**F**) cell viability. *$p < 0.05$, **$p < 0.01$, ***$p < 0.001$, and ****$p < 0.0001$, ns indicates no significant difference.

ability to induce apoptosis when contrasted with free Gen and LPs@Gen (Figure 8A and B). These results underscore the pivotal role of PLTM in augmenting anticancer efficacy.

Cell Targeting Ability of PLTM-LPs

To investigate whether PLTM-LPs can be specifically recruited into target cells in vitro, the uptake of PLTM-LPs-FITC by A549 cells and H1975 cells was observed using fluorescence microscopy. Figure 9A and C show that after incubation for 4 h, the green fluorescence of A549 and H1975 cells treated with free FITC was weak, and the fluorescence intensity of the two groups of cells treated with LPs-FITC was enhanced, while two cells treated with PLTM-LPs-FITC was significantly enhanced. In addition, the semiquantitative fluorescence results (Figure 9B and D) show that as the incubation time increased, the fluorescence values of each group of preparations in A549 and H1975 cells also rose, indicating that the intake of nanodrugs by tumor cells was time dependent. The fluorescence intensity of A549 and H1975 cells treated with PLTM-LPs-FITC was significantly higher than that in the Free FITC and LPs-FITC groups at all time points ($p < 0.01$). These results indicate that PLTM-LPs exhibits a greater affinity for lung cancer cells and is more readily internalized by tumor cells.

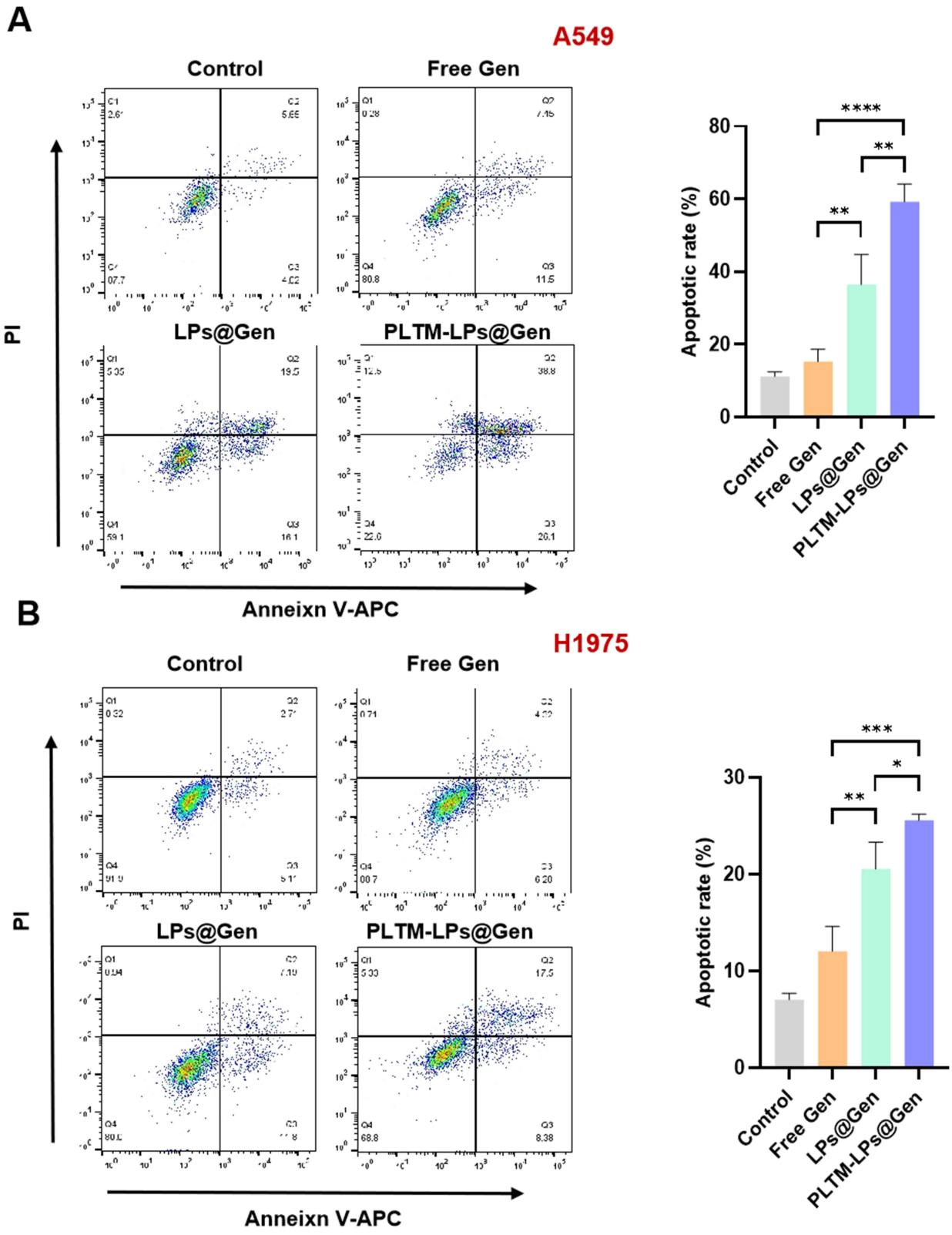

Figure 8 The effect of Gen preparations on apoptosis of A549 (**A**) and H1975 (**B**). *$p < 0.05$, **$p < 0.01$, ***$p < 0.001$, and ****$p < 0.0001$.

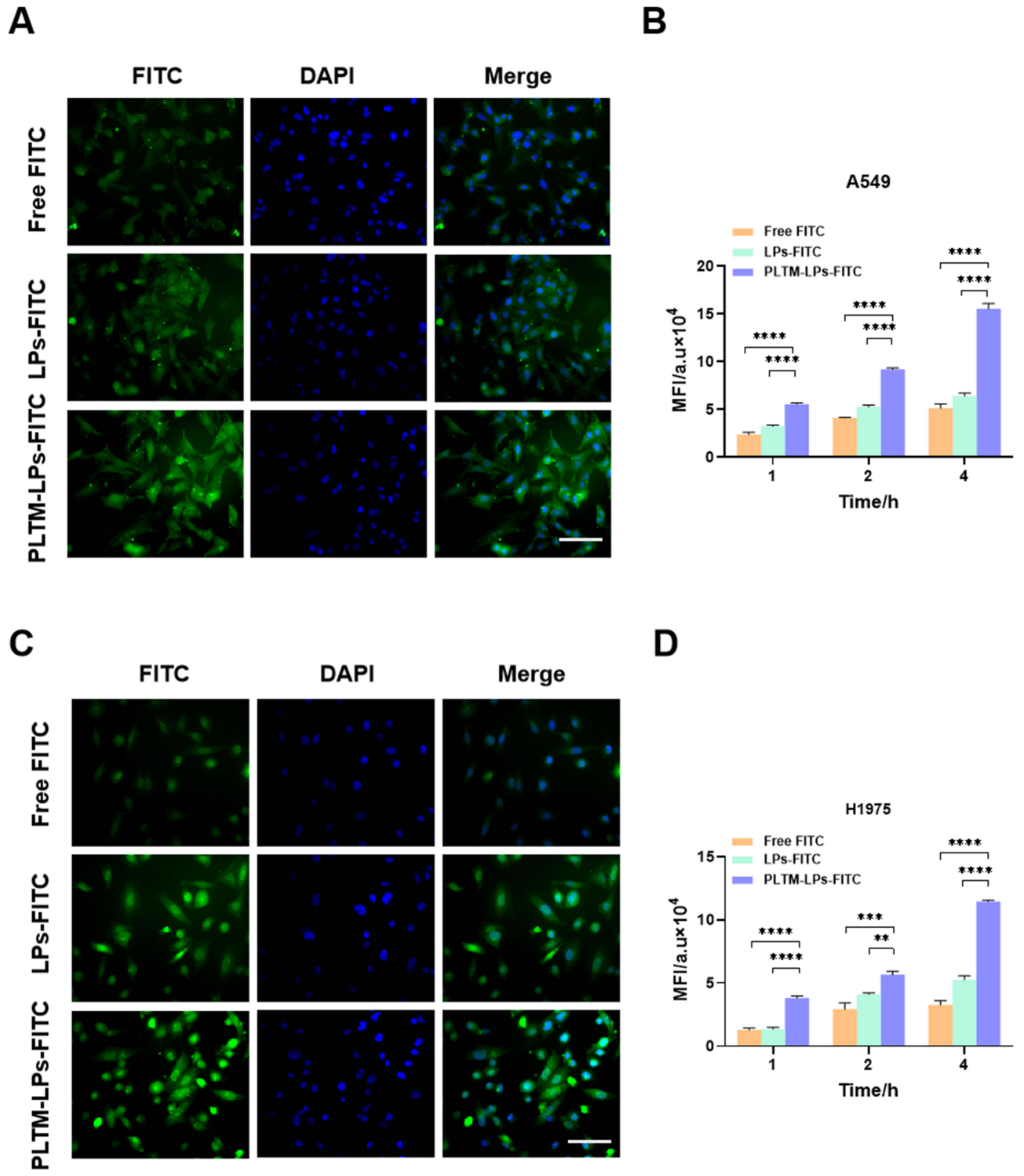

Figure 9 Uptake of A549 (**A** and **B**) and H1975 (**C** and **D**) to different preparation groups (scale bar, 50 μm), $^{**}p < 0.01$, $^{***}p < 0.001$, and $^{****}p < 0.0001$.

Immune Escape Ability of PLTM-LPs

To assess the immune escape ability of PLTM-LPs in vitro, the uptake capacity of macrophages to PLTM-LPs was investigated using fluorescence microscopy. The results from RAW264.7 cells treated with free FITC show evident green fluorescence (Figure 10A). In contrast, RAW264.7 cells treated with PLTM-LPs-FITC display only a weak green fluorescence signal compared to the Free FITC and LPs-FITC groups. The semiquantitative fluorescence results

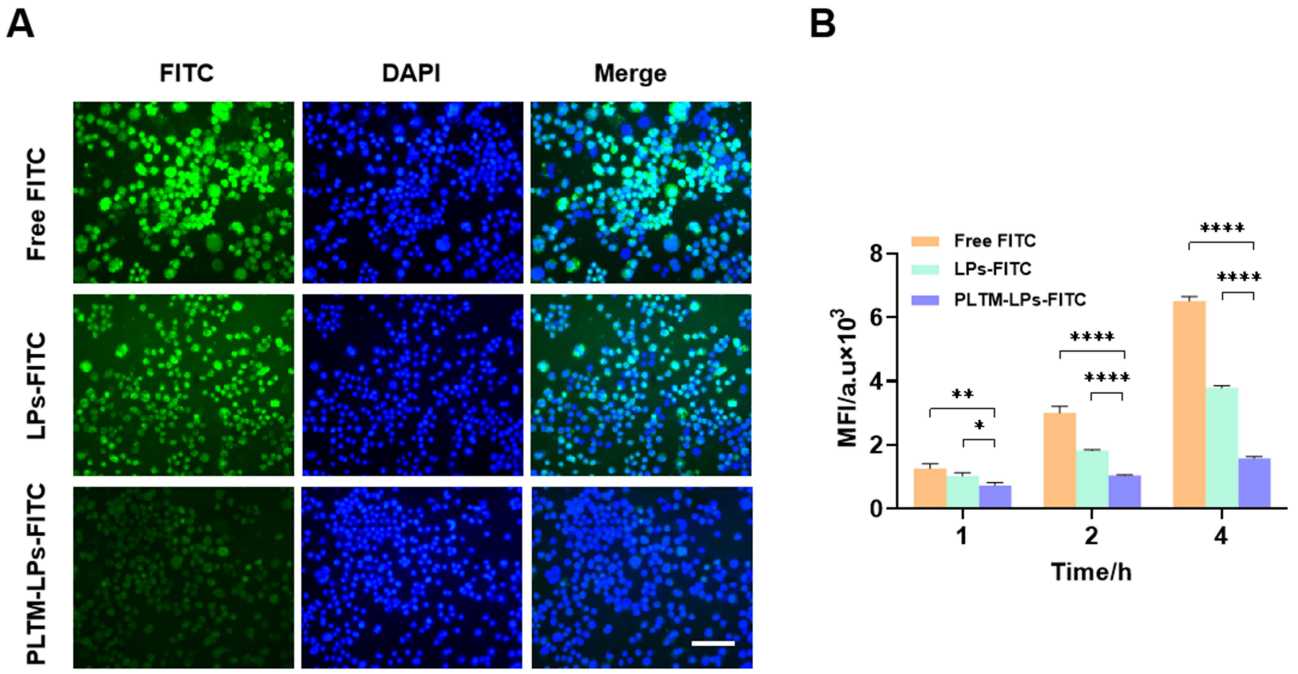

Figure 10 (**A**) Fluorescence micrographs uptake of different FITC preparations by RAW264.7 cells. (**B**) Mean fluorescence intensity of cellular uptake. (scale bar, 50 μm), *$p < 0.05$, **$p < 0.01$, and ****$p < 0.0001$.

(Figure 10B) indicate that the fluorescence value of the PLTM-LPs-FITC group was significantly lower than that of the Free FITC group and the LPs-FITC group at different time points ($p < 0.05$), indicating the phagocytosis of PLTM-LPs by macrophages was significantly weakened after PLTM chimerism. These results demonstrate the vector PLTM-LPs confers immune escape to the drug, potentially prolonging its the circulation time in vivo.

In vivo Targeting Ability of PLTM-LPs

After labeling LPs and PLTM-LPs with Cy5.5, the targeting effects of LPs-Cy5.5 and PLTM-LPs-Cy5.5 on tumor sites and metabolism of major organs were monitored via imaging in vivo. Figure 11A shows the fluorescence of the two carrier materials in the whole body of nude mice after the caudal vein injection for 1 h, which may be the distribution of NPs to the whole body after entering the blood circulation. After 6 h of injection, fluorescence was mainly observed in the liver and tumor sites, indicating LPs-Cy5.5 and PLTM-LPs-Cy5.5 could reach and accumulate in tumor lesions through blood circulation. By contrast, fluorescence in tumor sites of the PLTM-LPs-Cy5.5 group was significantly stronger than that of the LPs-Cy5.5 group. After 24 h of injection, the fluorescence signal of tumor sites of nude mice in all groups exhibited a decreasing trend. However, the fluorescence signal of tumor sites of nude mice in the LPs-Cy5.5 group was significantly weaker than that in the PLTM-LPs-Cy5.5 group at each time point. The results show PLTM modification can improve the stability of LPs in blood, prolong its circulation time in vivo, and increase the distribution of the drug in tumor lesions.

After 48 h of injection, the nude mice were euthanized, and the distribution of LPs-Cy5.5 and PLTM-LPs-Cy5.5 in tissues was detected by the imaging system of small animals. Figure 11B and C show that the fluorescence signals of the LPs-Cy5.5 group were mainly distributed in the liver and kidneys, while the PLTM-LPs-Cy5.5 group exhibited a primary distribution at tumor sites, with significantly lower accumulation in the liver and kidneys in comparison with the LPs-Cy5.5 group. These results further confirm that LPs can significantly improve its tumor targeting after mosaicism with PLTM.

In vivo Antitumor Effect of PLTM-LPs@Gen

Figure 12A shows the treatment protocol of PLTM-LPs@Gen for tumor-bearing nude mice. Tail vein administration was performed on day 10 after tumor cell inoculation (tumor size was about 100 mm^3). The tumor volume growth curve of tumor-bearing nude mice in each group is shown in Figure 12B. The Model control group exhibited a more rapid growth rate, and the

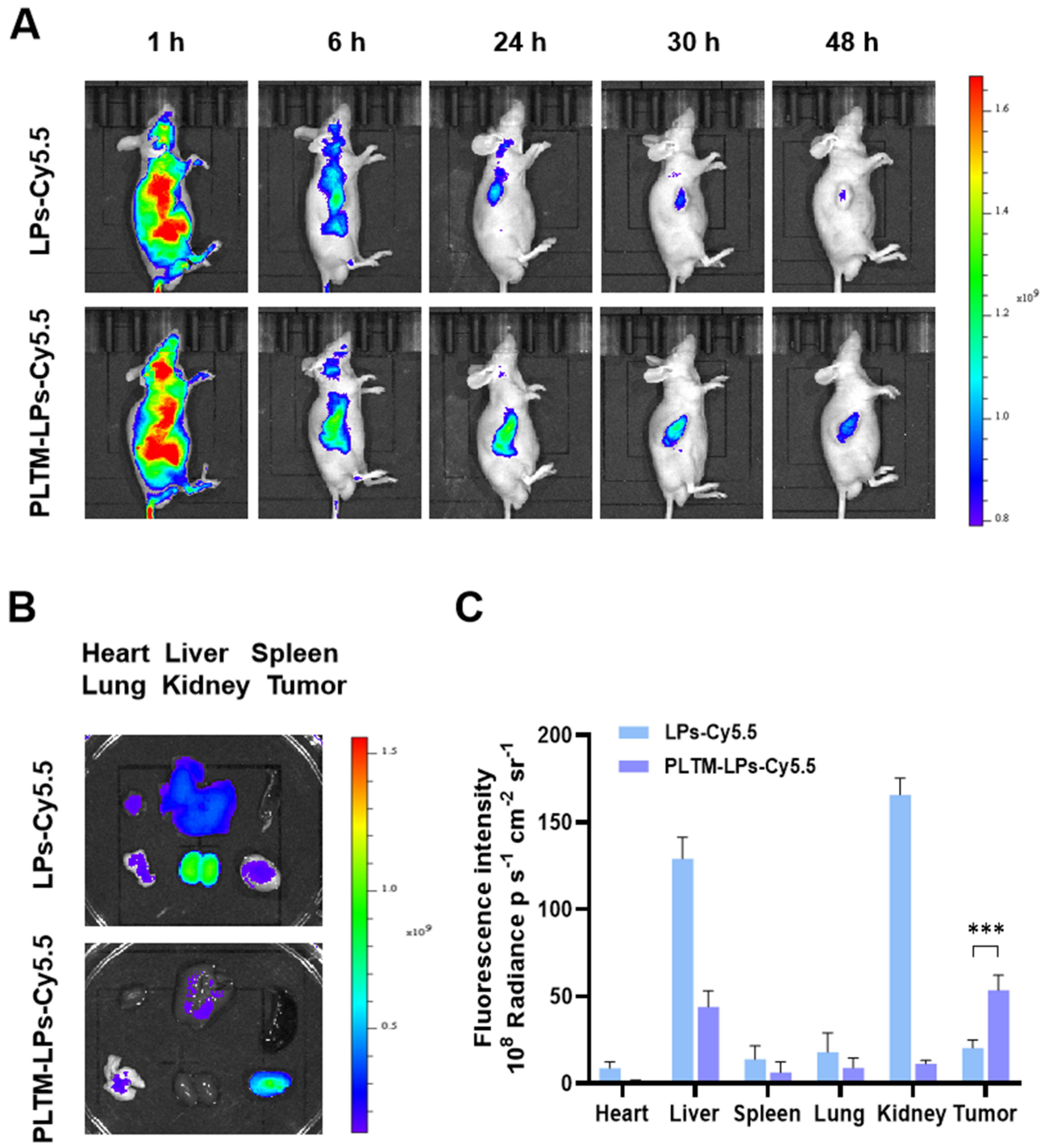

Figure 11 (**A**) In vivo fluorescence imaging after injection of fluorescently labeled material, (**B**) ex vivo fluorescence imaging, and (**C**) quantitative fluorescence statistics, ***$p < 0.001$.

tumor volume significantly increased in contrast to the initial measurement. The tumor volume growth in the three other drug administration groups was comparatively slow. In particular, the PLTM-LPs@Gen group had the slowest tumor growth, with significant differences compared with the other treated groups ($p < 0.05$). The tumor inhibition efficiency followed the order: PLTM-LPs@Gen > LPs@Gen > Free Gen. After administration, the tumor volume of nude mice showed that the Model control group's tumor volume was about 4.36 times greater than that of the PLTM-LPs@Gen group. When compared to the Free Gen group and the LPs@Gen group, the tumor inhibition efficiency of PLTM-LPs@Gen was increased by 2.43 and 1.44 times,

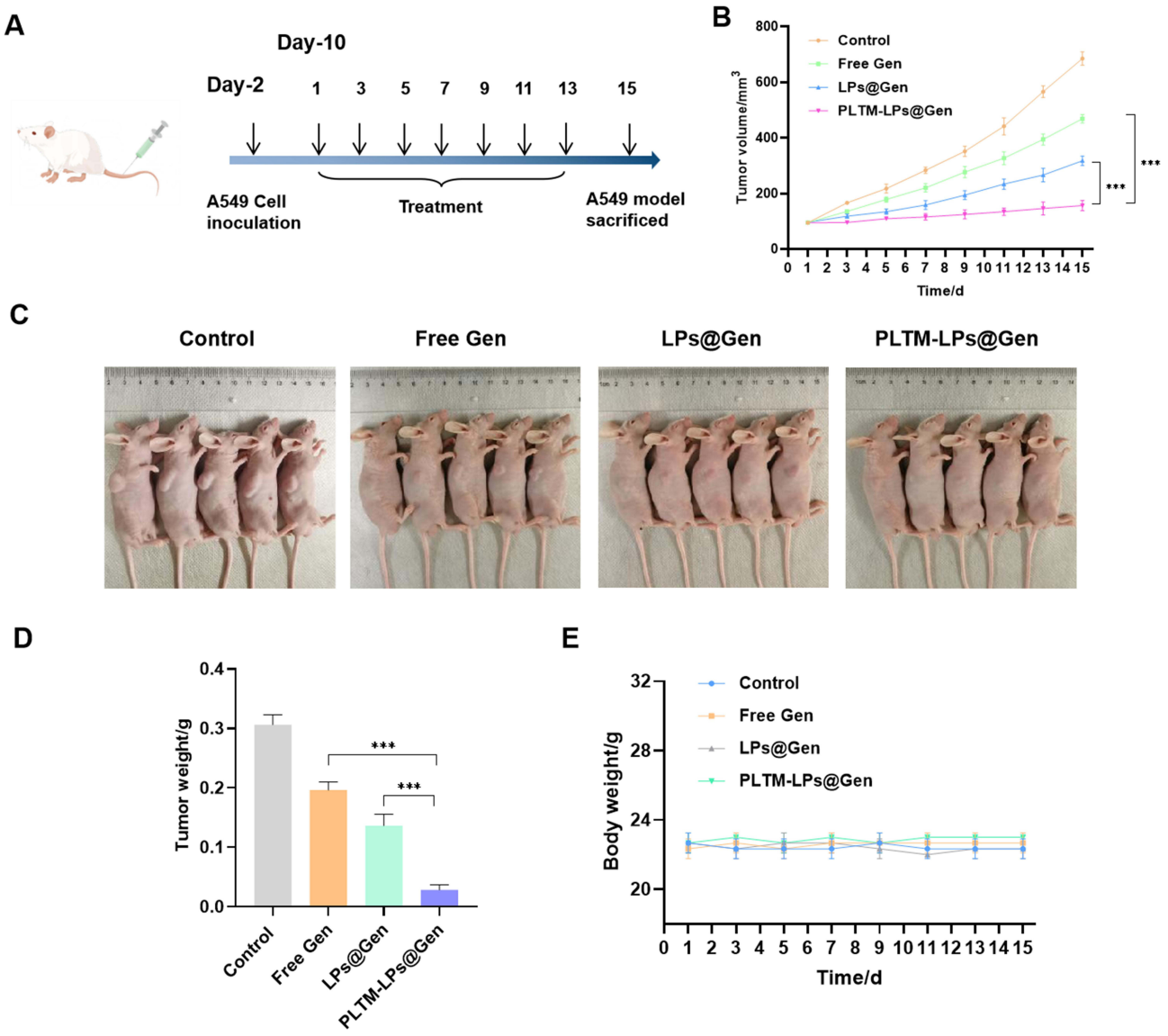

Figure 12 In vivo tumor suppression results of PLTM-LPs@Gen (n = 5). (**A**) Treatment time schematic. (**B**) Tumor growth curve. (**C**) In vivo tumor size comparison chart. (**D**) In vitro tumor mass weight comparison results. (**E**) Weight changes of nude mice in each group during treatment, ***$p < 0.001$.

respectively. The in vivo tumor results (Figure 12C) also visually show that the PLTM-LPs@Gen group had the most evident tumor inhibitory effect, which might be related to its greater enrichment in tumor sites.

After administration, the tumor masses of nude mice were weighed, and the results are shown in Figure 12D. The PLTM-LPs@Gen group reduced tumor weight to the greatest extent. The findings indicate that PLTM-LPs@Gen can significantly inhibit tumor growth, reflecting the best anti-lung cancer ability. Additionally, to evaluate the toxic effects and side effects of the preparations in each group, the body weight changes of nude mice during treatment were recorded. The results are displayed in Figure 12E. The body weight of all treatment groups remained stable during administration, and all nude mice showed active mental states during the whole treatment, indicating PLTM-LPs@Gen had minimal influence on the body weight changes of nude mice and was safe. This result may be attributed to the use of endogenous materials and exogenous materials with high biocompatibility.

H&E staining results of tumor tissues (Figure 13A) show that tumor cells in the Model control group were closely arranged with thickened nuclear membrane, while obvious tumor cell necrosis was observed in all treatment groups. Notably, in the PLTM-LPs@Gen group, irregular cell arrangement, cell shrinkage, chromatin concentration, and nucleus

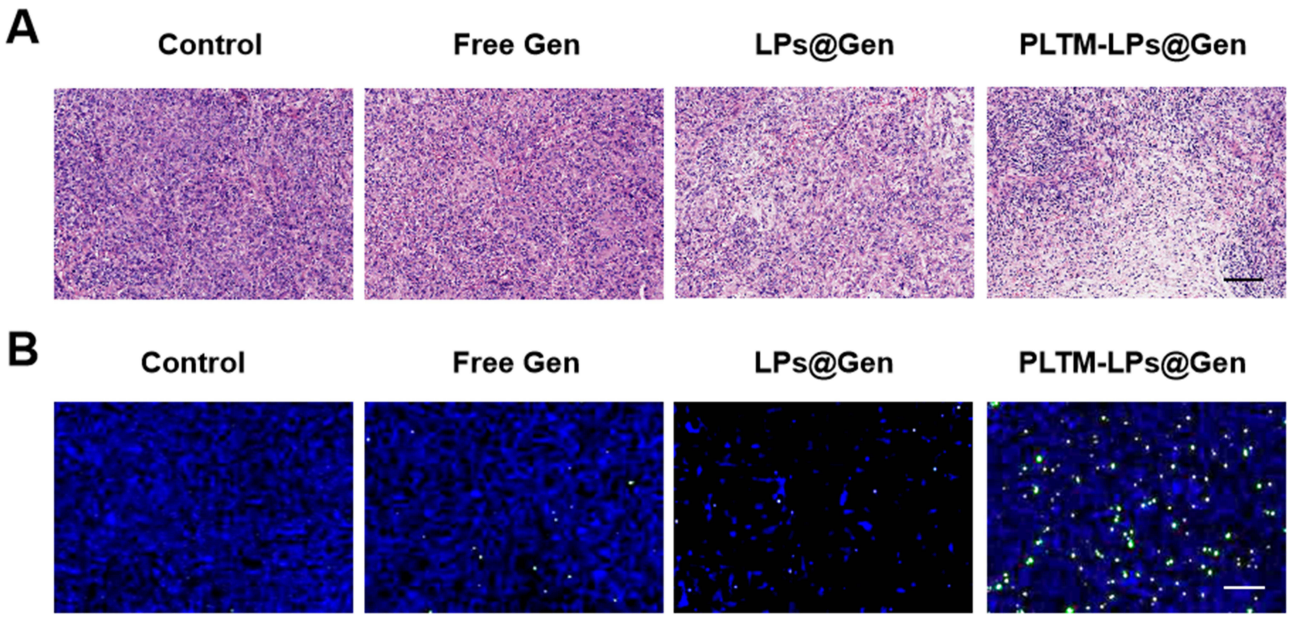

Figure 13 H&E (**A**) and TUNEL (**B**) results of tumor tissue sections (scale bar, 100 μm).

shrinkage could were evident, and the number of tumor cell necrosis was significantly higher than that in the Free Gen and LPs@Gen groups. TUNEL staining results (Figure 13B) show that almost no green fluorescence was observed in the Model control group, indicating little apoptosis of tumor cells, while different degrees of green fluorescence were observed in all treatment groups. Notably, the PLTM-LPs@Gen group exhibited the strongest green fluorescence signal in contrast to the Free Gen and LPs@Gen groups, indicating the highest incidence of tumor cell apoptosis. These results indicate that PLTM-LPs@Gen significantly promotes the necrosis and apoptosis of tumor cells.

Safety Evaluation of PLTM-LPs@Gen

To evaluate the potential of PLTM-LPs@Gen for biomedical applications further, its possible toxic side effects and biosafety concerns were examined. First, considering the tail vein administration mode, the toxicity of the carrier material PLTM-LPs and PLTM-LPs@Gen on HUVEC was investigated. The survival rate of HUVEC treated with PLTM-LPs was not significantly altered even when the concentration was up to 400 $\mu g \cdot mL^{-1}$ (Figure 14A). Interestingly, after PLTM-LPs@Gen treatment, the cell viability was increased evidently (Figure 14B), presenting Gen can promote HUVEC proliferation[43] and positively correlated with the Gen concentration. The above results emphasize the safety of bionic system. In addition, when incubated with red blood cells in vitro, the hemolysis rate of the PLTM-LPs@Gen group was much lower than that of the other groups. Even at the concentration as high as 2000 μM, the hemolysis rate remained only 1.14% (Figure 14C), indicating the constructed carrier does not readily induce hemolysis.

Platelets play a central role in clotting, and platelet particles contain substances related to clotting.[44] Therefore, whether PLTM-LPs@Gen caused blood clotting was investigated. The results show no significant difference in the coagulation indices TT and APTT of PLTM-LPs@Gen compared with the Normal control group (Figure 14D and E), indicating that nanopreparation does not easily cause coagulation and is safe in blood. This outcome may be attributed to the extracted PLTM, which does not exhibit a variety of binding sites for clotting factors. As a result, its affinity for these factors is low, leading to difficulty in clotting once it enters the body.

In addition, the toxicity of PLTM-LPs@Gen to major organs was investigated. In terms of liver and kidney function indices, no significant differences were observed among the four indices of the PLTM-LPs@Gen group compared to the Normal control group (Figure 14F–I), indicating it would not cause significant damage the liver or kidneys. This outcome was also proven by the results of organ H&E staining (Figure 15). The cells in the PLTM-LPs@Gen group were closely

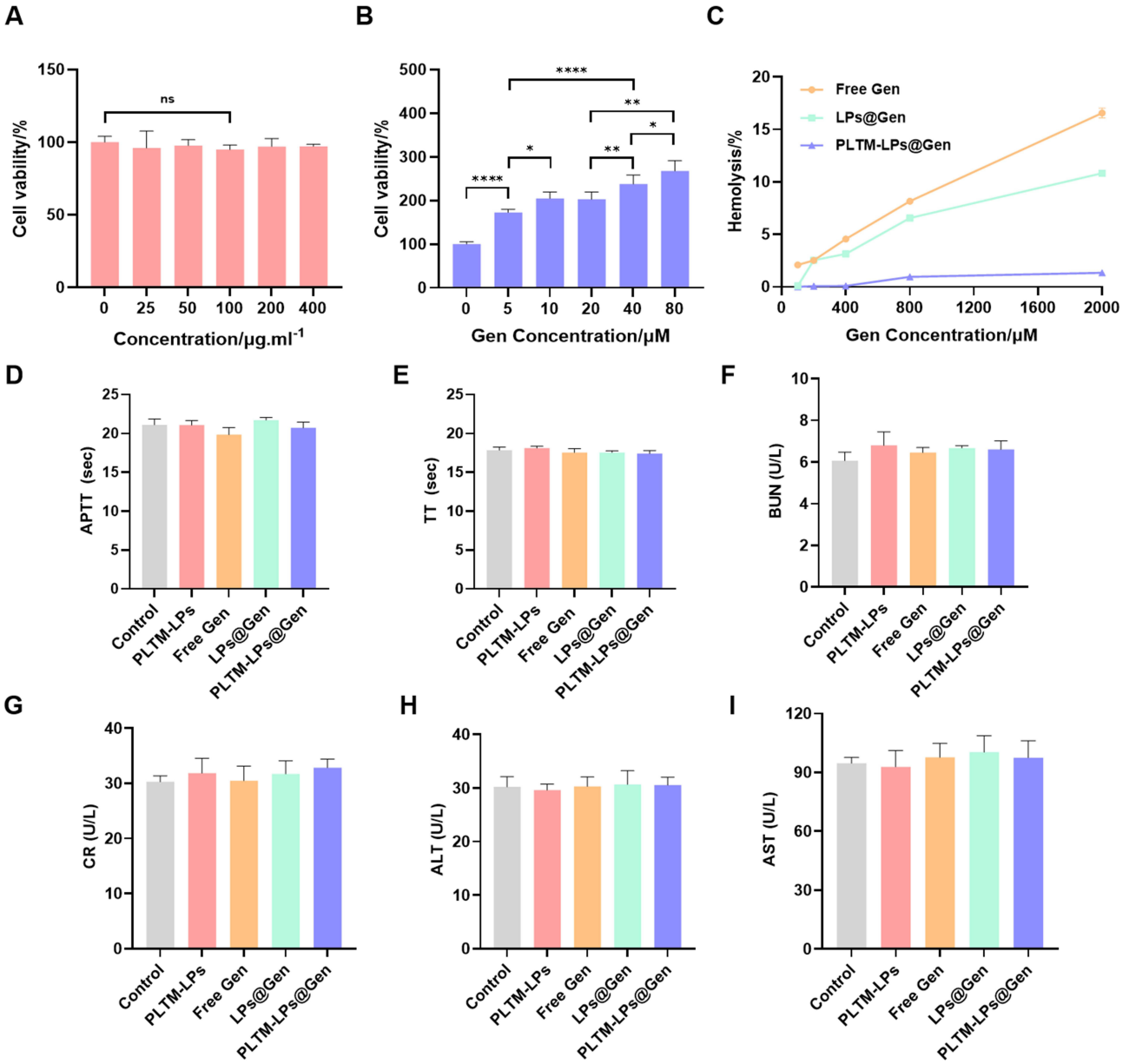

Figure 14 Effect of PLTM-LPs (**A**) and PLTM-LPs@Gen (**B**) on HUVEC viability. (**C**) Hemolysis results of the different preparations. (**D** and **E**) Effect of different preparation groups on in vivo coagulation indices of normal mice. (**F–I**) Effect of different preparation groups on serum biochemical indexes of normal mice (n = 3), *$p < 0.05$, **$p < 0.01$, ***$p < 0.001$, and ****$p < 0.0001$, ns indicates no significant difference.

arranged without evident damage, which was no different from the Normal control group. Therefore, the above results prove the high safety of the constructed bionic drug delivery system.

Discussion

Recently, natural products have garnered attention as potential anticancer drugs due to their unique biological activities and sustainability. Among these, Gen has demonstrated significant inhibitory effects on lung cancer cells. However, as an insoluble drug, Gen exhibits low bioavailability in vivo, making it difficult to accumulate in the target site, thus leading to its limited application in clinical practice. To address these challenges, this study used LPs to encapsulate Gen within a phospholipid bilayer. Additionally, we fused PLTM with LPs@Gen to create the biomimetic drug delivery, PLTM-LPs@Gen.

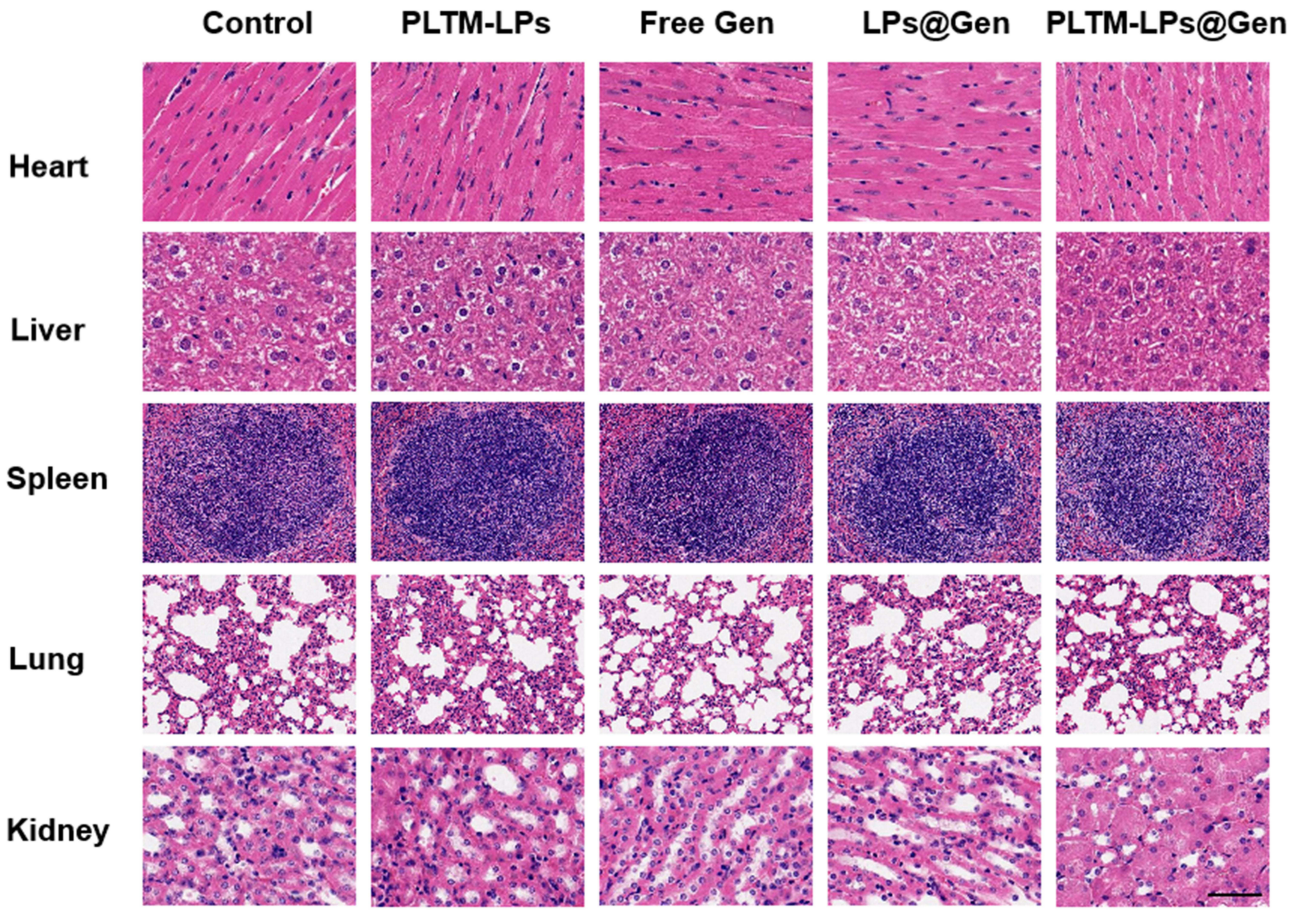

Figure 15 H&E of different Gen preparations and carrier material on major organs of normal mice (scale bar, 100 μm).

SL and CHO were used as the lipid materials in this LPs prescription, because they are highly biocompatible and approved by the FDA and have been used in the marketed LPs products.[45] However, LPs@Gen prepared from SL and CHO was prone to precipitate due to poor stability. DSPE-PEG2000 is able to encapsulate in the polar groups of LPs in the form of covalent bonds, promoting vesicle formation and thus preventing drug leakage.[46] Therefore, to enhance the stability of the formulation, DSPE-PEG2000 was incorporated. In addition, as a functionalized polyethylene glycol material, DSPE-PEG2000 possesses a prolonged circulation capability, which significantly improves the blood circulation time of drugs, thereby enabling the nanopreparations the ability to passively target tumors.[47]

The efficient fusion of PLTM and LPs@Gen is a critical step in the preparation of PLTM-LPs@Gen. In this study, the optimal fusion ratio of the two components was determined to be 1:1 through colocalization screening, which was also confirmed by Sun et al.[48] However, the targeting ability of PLTM-LPs@Gen is associated with the amount of membrane protein, so it is essential to evaluate the in vitro and in vivo targeting effect of PLTM-LPs@Gen obtained at different ratios of the two to further determine the optimal fusion ratio to achieve the therapeutic effect.

The state and location of the drug within NPs significantly influence drug release. Drugs can be encapsulated within NPs, adsorbed onto their surfaces, or located in the surface or shell of the NPs, leading to variations in the drug release rate.[49] In this study, the drug release in the PLTM-LPs@Gen group showed a biphasic phenomenon when compared with the Free Gen group. The "burst release" within 0–4 h may be attributed to some drugs being adsorbed onto the nanosurface without being fully encapsulated. After 4 h, the drug encapsulated in PLTM-LPs may be released from the carrier and subsequently enter the release medium through the dialysis bag.

In vitro and in vivo experiments demonstrate that PLTM-LPs@Gen exhibits superior targeting and immune escape capabilities. PLTM-LPs-FITC was able to be ingested more by tumor cells than in the Free FITC and LPs-FITC groups,

which may result from the interaction of CD44 receptor highly expressed on the surface of lung cancer cells with CD62p protein on PLTM. CD44 protein is a transmembrane glycoprotein, and recent studies have shown that it plays a significant role in the initiation and progression of tumors.[50] The abundant CD62p on the surface of PLTM specifically binds to the CD44 protein on the surface of tumor cells, facilitating the accumulation of drugs at tumor sites. Lipid NPs efficiently deliver their contents to target cells through membrane fusion, thereby regulating the function of these cells. Wang et al[51] also found that the PLTM coated bufalin PLGA NP exhibited a significantly higher uptake efficiency by H22 liver cancer cells because CD62p on the surface of PLTM could be targeted to bind to the CD44 receptor of H22 liver cancer cells. The cellular uptake efficiency of PLTM coated bufalin NP was about 7.4 times higher than that of uncoated bufalin NP. Additionally, the in vivo biodistribution results indicated that the accumulation of PLTM-LPs at the tumor site was significantly higher than that of LPs not coated with PLTM. Hu et al[41] also confirmed that polymer NPs coated with PLTM can effectively target the bone microenvironment and myeloma cells. In summary, PLTM enhances the ability of delivery systems to target tumors, which is crucial for improving therapeutic efficacy. As previously mentioned, PLTM disguised nanomaterials retain the proteins of the protomembrane, including CD47, which signals "Don't eat me" to macrophages.[52] Consequently, the phagocytosis of macrophages to LPs@Gen coated with PLTM was significantly reduced. Jing et al[53] found that, compared to conventional preparation, the uptake rate of adriamycin by RAW264.7 cells was decreased by 67.5% after coating adriamycin with PLTM, which significantly enhanced the immune escape capability. This finding was further corroborated by the in vitro immune escape results and in vivo distribution results in this study.

In vitro cytotoxicity assays demonstrate a time-dependent growth inhibition of PLTM-LPs@Gen on the A549 and H1975 cells. At 2 h, the inhibition rate of PLTM-LPs@Gen on A549 cells was not significantly different from that of free Gen, which may be attributed to the slow release of Gen from the NPs. At 8 and 24 h, the inhibition rate of PLTM-LPs @Gen was significantly higher than that of LPs@Gen, likely due to the interaction between PLTM proteins and CD44 in lung cancer cells. Ying et al[54] found that the inhibition rate of camptothecin on breast cancer cells increased by 3.9 times when encapsulated in a macrophage membrane, suggesting that bionic technology could be used to improve the efficacy of anticancer drugs. Furthermore, the results regarding cell viability and apoptosis demonstrate that PLTM significantly improves the therapeutic efficacy of LPs@Gen. Additionally, the carrier material PLTM-LPs exhibited no significant cytotoxic effects on A549 and H1975 cells, indicating that PLTM-LPs can be considered a relatively safe drug carrier. The tumor suppression rate is a crucial indicator for evaluating the effectiveness of the preparation in vivo efficacy assessments. The PLTM-LPs@Gen treatment group significantly inhibited tumor cell proliferation and reduced both the weight and volume of tumors in nude mice, further indicating that PLTM-LPs@Gen is a highly effective biomimetic nanoplatform for the treatment of lung cancer.

To evaluate the safety of the biomimetic drug delivery system, its biosafety was analyzed both in vitro and in vivo. Given that the administration method of the preparation is tail vein injection, HUVEC was selected as the model cell to evaluate the cytotoxicity of the carrier material. The results show that the carrier material did not significantly inhibit the activity of HUVEC. Liu et al[31] also found that LP carriers in biomimetic cell membranes exhibit lower toxicity to normal HUVEC. Consistent with previous studies,[55] Gen promoted the proliferation of HUVEC, suggesting potential cardiovascular protective effects. Blood compatibility is affected by the injection of NPs directly into the systemic circulation.[56] An in vitro hemolysis test demonstrated that PLTM-LPs@Gen exhibited high blood compatibility and did not induce significant hemolysis of red blood cells. Furthermore, the systemic toxicity of PLTM-LPs@Gen was assessed in relation to blood and organ health, and the biosafety evaluation results indicate no significant toxicity associated with PLTM-LPs@Gen. In conclusion, PLTM-LPs@Gen demonstrates good biocompatibility and serves as a safe platform for antitumor therapy.

Conclusions

This paper successfully constructed a bionic NP drug delivery system, PLTM-LPs@Gen, which disguised by natural material PLTM. The in vitro and in vivo experimental results show that the bionic carrier significantly enhanced the antitumor efficiency of drugs without evident toxic effects. The reason may be that PLTM-LPs@Gen can simulate platelets to specifically send an "Eat me" signal to tumor cells, thus "inducing" tumor cells to "eat" anticancer drugs, to improve potentially the active targeting ability of drugs to tumors. Additionally, PLTM-LPs@Gen can emit a "Don't eat me" signal

to macrophages to prevent the drug delivery system from being recognized and cleared by the reticuloendothelial system, potentially extending the circulation time of drugs in the body, thereby enhancing the passive targeting ability of drugs. In summary, the bionic drug delivery system effectively enhances drug efficacy while minimizing toxic side effects. This bionic strategy holds potential advantages and clinical transformation prospects for targeted therapy of various types of tumors, including lung cancer.

Acknowledgments

We gratefully acknowledge the assistance of Key Discipline of Zhejiang Province in Public Health and Preventive Medicine (First Class, Category A), Hangzhou Medical College.

Funding

This work was supported by the Huadong Medicine Joint Funds of the Zhejiang Provincial Natural Science Foundation of China [No. LHDMZ22H300009], Key Research Projects of Hangzhou Medical College [No. KYZD202106], Key Laboratory of Neuropsychiatric Drug Research of Zhejiang Province [No.2019E10021], Zhejiang Provincial Public Welfare Program [LGN22H280009, LTGN23H280003], Zhejiang Provincial Drug Administration Science and Technology Plan Project [2022008], and Ningbo Public Welfare Program [2023S058].

Disclosure

The authors report no conflicts of interest in this work.

References

1. Siegel RL, Miller KD. Cancer statistics, 2023. *CA Cancer J Clin*. 2023;73(1):17–48. doi:10.3322/caac.21763
2. Sung H, Ferlay J, Siegel RL. Global Cancer Statistics 2020: GLOBOCAN Estimates of Incidence and Mortality Worldwide for 36 Cancers in 185 Countries. *CA Cancer J Clin*. 2021;71(3):209–249. doi:10.3322/caac.21660
3. Lahiri A, Maji A, Potdar PD, et al. Lung cancer immunotherapy: progress, pitfalls, and promises. *Mol Canc*. 2023;22(1):40.10.1186/s12943–023–01740–y.
4. Provencio M, Calvo V, Romero A, Spicer JD, Cruz-Bermúdez A. Treatment Sequencing in Resectable Lung Cancer: the Good and the Bad of Adjuvant Versus Neoadjuvant Therapy. *Am Soc Clin Oncol Educ Book*. 2022;42(1):18. doi:10.1200/edbk_358995
5. El-Hussein A, Manoto SL, Ombinda-Lemboumba S, Alrowaili ZA, Mthunzi-Kufa P. A Review of Chemotherapy and Photodynamic Therapy for Lung Cancer Treatment. *Anticancer Agents Med Chem*. 2021;21(2):149–161. doi:10.2174/1871520620666200403144945
6. Ruiz-Cordero R, Devine WP. Targeted Therapy and Checkpoint Immunotherapy in Lung Cancer. *Surg Pathol Clin*. 2020;13(1):17–33. doi:10.1016/j.path.2019.11.002
7. Yu X, Yan J, Li Y, et al. Inhibition of castration-resistant prostate cancer growth by genistein through suppression of AKR1C3. *Food Nutr Res*. 2023;67:9024. doi:10.29219/fnr.v67.9024
8. Pawlicka MA, Zmorzyński S, Popek-Marciniec S. The Effects of Genistein at Different Concentrations on MCF-7 Breast Cancer Cells and BJ Dermal Fibroblasts. *Int J Mol Sci*. 2022;23(20):12360. doi:10.3390/ijms232012360
9. Javed Z, Khan K, Herrera-Bravo J, et al. Genistein as a regulator of signaling pathways and microRNAs in different types of cancers. *Cancer Cell Int*. 2021;21(1):388. doi:10.1186/s12935-021-02091-8
10. Sacko K, Thangavel K, Shoyele SA. Codelivery of Genistein and miRNA-29b to A549 Cells Using Aptamer-Hybrid Nanoparticle Bioconjugates. *Nanomaterials*. 2019;9(7):1052. doi:10.3390/nano9071052
11. Yu Y, Xing Y, Zhang Q, et al. Soy isoflavone genistein inhibits hsa_circ_0031250/miR-873-5p/FOXM1 axis to suppress non-small-cell lung cancer progression. *IUBMB Life*. 2021;73(1):92–107. doi:10.1002/iub.2404
12. Zhu H, Cheng H, Ren Y, Liu ZG, Zhang YF, De Luo B. Synergistic inhibitory effects by the combination of gefitinib and genistein on NSCLC with acquired drug-resistance in vitro and in vivo. *Mol Biol Rep*. 2012;39(4):4971–4979. doi:10.1007/s11033-011-1293-1
13. Jangid AK, Solanki R, Patel S, Pooja D, Kulhari H. Genistein encapsulated inulin-stearic acid bioconjugate nanoparticles: formulation development, characterization and anticancer activity. *Int J Biol Macromol*. 2022;206:213–221. doi:10.1016/j.ijbiomac.2022.02.031
14. Kwon SH, Kim SY, Ha KW, et al. Pharmaceutical evaluation of genistein-loaded pluronic micelles for oral delivery. *Arch Pharm Res*. 2007;30(9):1138–1143. doi:10.1007/bf02980249
15. Zhang T, Wang H, Ye Y, Zhang X, Wu B. Micellar emulsions composed of mPEG-PCL/MCT as novel nanocarriers for systemic delivery of genistein: a comparative study with micelles. *Int J Nanomed*. 2015;10:6175–6184. doi:10.2147/ijn.s91348
16. Qiu Z, Yu Z, Xu T, et al. Novel Nano-Drug Delivery System for Brain Tumor Treatment. *Cells*. 2022;11(23):3761. doi:10.3390/cells11233761
17. Aditya NP, Shim M, Lee I, Lee Y, Im MH, Ko S. Curcumin and genistein coloaded nanostructured lipid carriers: in vitro digestion and antiprostate cancer activity. *J Agric Food Chem*. 2013;61(8):1878–1883. doi:10.1021/jf305143k
18. Cai L, Yu R, Hao X, Ding X. Folate Receptor-targeted Bioflavonoid Genistein-loaded Chitosan Nanoparticles for Enhanced Anticancer Effect in Cervical Cancers. *Nanoscale Res Lett*. 2017;12(1):509.10.1186/s11671–017–2253–z.
19. Sercombe L, Veerati T, Moheimani F, Wu SY, Sood AK, Hua S. Advances and Challenges of Liposome Assisted Drug Delivery. *Front Pharmacol*. 2015;6:286. doi:10.3389/fphar.2015.00286

20. Zhang M, Lou C, Cao A. Progresses on active targeting liposome drug delivery systems for tumor therapy. *J Biomed Eng*. 2022;39(3):633–638. doi:10.7507/1001-5515.202110067
21. Cheng Z, Li M, Dey R, Chen Y. Nanomaterials for cancer therapy: current progress and perspectives. *J Hematol Oncol*. 2021;14(1):85. doi:10.1186/s13045-021-01096-0
22. Fan Y, Zhou Y, Lu M, Si H, Li L, Tang B. Responsive Dual-Targeting Exosome as a Drug Carrier for Combination Cancer Immunotherapy. *Research*. 2021;2021:9862876. doi:10.34133/2021/9862876
23. Mao L, Jiang Y, Ouyang H, Feng Y, Li R, Zhang X. Revealing the Distribution of Aggregation-Induced Emission Nanoparticles via Dual-Modality Imaging with Fluorescence and Mass Spectrometry. *Research*. 2021;2021:9784053. doi:10.34133/2021/9784053
24. Fang RH, Kroll AV, Gao W, Zhang L. Cell Membrane Coating Nanotechnology. *Adv Mater*. 2018;30(23):e1706759. doi:10.1002/adma.201706759
25. Fang RH, Gao W, Zhang L. Targeting drugs to tumours using cell membrane-coated nanoparticles. *Nat Rev Clin Oncol*. 2023;20(1):33–48. doi:10.1038/s41571-022-00699-x
26. Nie D, Dai Z, Li J, et al. Cancer-Cell-Membrane-Coated Nanoparticles with a Yolk-Shell Structure Augment Cancer Chemotherapy. *Nano Lett*. 2020;20(2):936–946. doi:10.1021/acs.nanolett.9b03817
27. Geranpayehvaghei M, Dabirmanesh B, Khaledi M, et al. Cancer-associated-platelet-inspired nanomedicines for cancer therapy. *Wiley Interdiscip Rev Nanomed Nanobio*. 2021;13(5):e1702. doi:10.1002/wnan.1702
28. Ma Q, Fan Q, Xu J, et al. Calming Cytokine Storm in Pneumonia by Targeted Delivery of TPCA-1 Using Platelet-Derived Extracellular Vesicles. *Matter*. 2020;3(1):287–301. doi:10.1016/j.matt.2020.05.017
29. Chen YQ, Zhu WT, Lin CY, Yuan ZW. Delivery of Rapamycin by Liposomes Synergistically Enhances the Chemotherapy Effect of 5-Fluorouracil on Colorectal Cancer. *Int J Nanomed*. 2021;16:269–281. doi:10.2147/ijn.s270939
30. Jin H, Li J, Zhang M, et al. Berberine-Loaded Biomimetic Nanoparticles Attenuate Inflammation of Experimental Allergic Asthma via Enhancing IL-12 Expression. *Front Pharmacol*. 2021;12:724525. doi:10.3389/fphar.2021.724525
31. Liu G, Zhao X, Zhang Y, et al. Engineering Biomimetic Platesomes for pH-Responsive Drug Delivery and Enhanced Antitumor Activity. *Adv Mater*. 2019;31(32):e1900795. doi:10.1002/adma.201900795
32. Wu Y, Fan Q, Zhou J, et al. Biomimetic platelet-like nanoparticles enhance targeted hepatocellular carcinoma therapy. *Colloids Surf B*. 2024;240:113973. doi:10.1016/j.colsurfb.2024.113973
33. Gao C, Lin Z, Jurado-Sánchez B, Lin X, Wu Z, He Q. Stem Cell Membrane-Coated Nanogels for Highly Efficient In Vivo Tumor Targeted Drug Delivery. *Small*. 2016;12(30):4056–4062. doi:10.1002/smll.201600624
34. Shen H, He D, Wang S, Ding P, Wang J. Preparation, characterization, and pharmacokinetics study of a novel genistein-loaded mixed micelles system. *Drug Dev Ind Pharm*. 2018;44(9):1536–1542. doi:10.1080/03639045.2018.1483384
35. Xu H, Ma H, Zha L, Li Q, Pan H, Zhang L. Genistein promotes apoptosis of lung cancer cells through the IMPDH2/AKT1 pathway. *Am J Transl Res*. 2022;14(10):7040–7051.
36. Wang X, Gao X, Tian J, et al. LINC00261 inhibits progression of pancreatic cancer by down-regulating miR-23a-3p. *Arch Biochem Biophys*. 2020;689:108469. doi:10.1016/j.abb.2020.108469
37. Wan S, Fan Q, Wu Y, et al. Curcumin-Loaded Platelet Membrane Bioinspired Chitosan-Modified Liposome for Effective Cancer Therapy. *Pharmaceutics*. 2023;15(2):631. doi:10.3390/pharmaceutics15020631
38. Wen Q, Zhang Y, Muluh TA, et al. Erythrocyte membrane-camouflaged gefitinib/albumin nanoparticles for tumor imaging and targeted therapy against lung cancer. *Inter J Biol Macromol*. 2021;193(Pt A):228–237. doi:10.1016/j.ijbiomac.2021.10.113
39. Song Y, He Y, Rong L, et al. "Platelet-coated bullets" biomimetic nanoparticles to ameliorate experimental colitis by targeting endothelial cells. *Biomater Adv*. 2023;148:213378. doi:10.1016/j.bioadv.2023.213378
40. Tatsuta M, Iishi H, Baba M, Yano H, Uehara H, Nakaizumi A. Attenuation by genistein of sodium-chloride-enhanced gastric carcinogenesis induced by N-methyl-N'-nitro-N-nitrosoguanidine in Wistar rats. *Int J Cancer Jan*. 1999;80(3):396–399. doi:10.1002/(sici)1097-0215(19990129)80:3<396::aid-ijc10>3.0.co;2-1
41. Bardania H, Shojaosadati SA, Kobarfard F, et al. RGD-Modified Nano-Liposomes Encapsulated Eptifibatide with Proper Hemocompatibility and Cytotoxicity Effect. *Iran J Biotechnol Apr*. 2019;17(2):e2008. doi:10.21859/ijb.2008
42. Chan L, Pang Y, Wang Y, et al. Genistein-induced mitochondrial dysfunction and FOXO3a/PUMA expression in non-small lung cancer cells. *Pharm Biol*. 2022;60(1):1876–1883. doi:10.1080/13880209.2022.2123933
43. Wu G, Li S, Qu G, et al. Genistein alleviates H(2)O(2)-induced senescence of human umbilical vein endothelial cells via regulating the TXNIP/NLRP3 axis. *Pharm Biol*. 2021;59(1):1388–1401. doi:10.1080/13880209.2021.1979052
44. Mandel J, Casari M. Beyond Hemostasis: platelet Innate Immune Interactions and Thromboinflammation. *Int J Mol Sci*. 2022;23(7):3868. doi:10.3390/ijms23073868
45. Barenholz Y. Doxil®–the first FDA-approved nano-drug: lessons learned. *J Control Release*. 2012;160(2):117–134. doi:10.1016/j.jconrel.2012.03.020
46. Chen Y, Chen J, Cheng Y, et al. A lyophilized sterically stabilized liposome-containing docetaxel: in vitro and in vivo evaluation. *J Liposome Res*. 2017;27(1):64–73. doi:10.3109/08982104.2016.1158185
47. Wang Z, Ling L, Du Y, Yao C, Li X. Reduction responsive liposomes based on paclitaxel-ss-lysophospholipid with high drug loading for intracellular delivery. *Int J Pharm*. 2019;564:244–255. doi:10.1016/j.ijpharm.2019.04.060
48. Sun T, Kwong CHT, Gao C, et al. Amelioration of ulcerative colitis via inflammatory regulation by macrophage-biomimetic nanomedicine. *Theranostics*. 2020;10(22):10106–10119. doi:10.7150/thno.48448
49. Mitchell MJ, Billingsley MM, Haley RM. Engineering precision nanoparticles for drug delivery. *Nat Rev Drug Discov*. 2021;20(2):101–124. doi:10.1038/s41573-020-0090-8
50. Xu H, Niu M, Yuan X, Wu K, Liu A. CD44 as a tumor biomarker and therapeutic target. *Exp Hematol Oncol*. 2020;9(1):36. doi:10.1186/s40164-020-00192-0
51. Wang H, Wu J, Williams GR, et al. Platelet-membrane-biomimetic nanoparticles for targeted antitumor drug delivery. *J Nanobiotechnology*. 2019;17(1):60.10.1186/s12951–019–0494–y.
52. Alvey C, Discher DE. Engineering macrophages to eat cancer: from "marker of self" CD47 and phagocytosis to differentiation. *J Leukoc Biol*. 2017;102(1):31–40. doi:10.1189/jlb.4RI1216-516R

53. Jing L, Qu H, Wu D, et al. Platelet-camouflaged nanococktail: simultaneous inhibition of drug-resistant tumor growth and metastasis via a cancer cells and tumor vasculature dual-targeting strategy. *Theranostics*. 2018;8(10):2683–2695. doi:10.7150/thno.23654
54. Ying K, Zhu Y, Wan J, et al. Macrophage membrane-biomimetic adhesive polycaprolactone nanocamptothecin for improving cancer-targeting efficiency and impairing metastasis. *Bioact Mater*. 2023;20:449–462. doi:10.1016/j.bioactmat.2022.06.013
55. Li H, Zhang Q. Research Progress of Flavonoids Regulating Endothelial Function. *Pharmaceuticals*. 2023;16(9). doi:10.3390/ph16091201
56. Guimarães D, Cavaco-Paulo A, Nogueira E. Design of liposomes as drug delivery system for therapeutic applications. *Int J Pharm*. 2021;601:120571. doi:10.1016/j.ijpharm.2021.120571